Grid-Based Hydrodynamics in Astrophysical Fluid Flows

Romain Teyssier

University of Zurich, Institute for Computational Science, Center for Theoretical Astrophysics and Cosmology, CH-8057 Zurich; email: teyssier@physik.uzh.ch

Annu. Rev. Astron. Astrophys. 2015. 53:325–64

First published online as a Review in Advance on June 18, 2015

The *Annual Review of Astronomy and Astrophysics* is online at astro.annualreviews.org

This article's doi: 10.1146/annurev-astro-082214-122309

Keywords

conservation laws, gas dynamics, magnetohydrodynamics, radiation, numerical simulations

Abstract

In this review, the equations of hydrodynamics, magnetohydrodynamics, and radiation hydrodynamics are presented, together with their corresponding nonideal source terms. I overview the current landscape of modern grid-based numerical techniques with an emphasis on numerical diffusion, which plays a fundamental role in stabilizing the solution but is also the main source of errors associated with these numerical techniques. I discuss in great detail the inclusion of additional important source terms, such as cooling and gravity. I also show how to modify classic operator-splitting techniques to avoid undesirable numerical errors associated with these additional source terms, in particular in the presence of highly supersonic flows. I finally present various mesh adaptation strategies that can be used to minimize these numerical errors. To conclude, I review existing astrophysical software that is publicly available to perform simulations for such astrophysical fluids.

1. INTRODUCTION

Numerical hydrodynamics has been playing a central role in theoretical astrophysics since the early fifties and the first shock-clouds interaction simulations. It is also very popular in natural sciences in general, like climate research and weather modeling. Astrophysics represents a particular challenge for computational fluid dynamics (CFD), as it addresses very specific problems that are quite far from traditional fluid dynamics. Numerical techniques were developed in the late 80s, leading to the design of very popular and powerful numerical codes for astrophysical fluid dynamics. The ZEUS code stood out as one of the most popular grid-based hydrodynamics codes in the late 80s, using simple finite difference schemes (Stone et al. 1992; Stone & Norman 1992a,b) and, roughly at the same time, the Monotonic Upstream-Centered Scheme for Conservations Laws (MUSCL) scheme (van Leer 1976) and the Piecewise Parabolic Method (Colella & Woodward 1984) appeared as the first viable implementations of high-order Godunov schemes. More than 20 years later, it is timely to review the current status of this developing field, but I restrict discussion to the case of compressible fluid flows. Incompressible or anelastic flows, such as stellar interiors, or collisionless fluids, such as dark matter haloes, are not discussed but presented elsewhere. The associated numerical techniques, usually spectral methods for the former (Gottlieb et al. 1978) and particle-based techniques for the latter (Hockney & Eastwood 1988), are also ignored in this review. For a review on another very popular numerical technique for fluids, namely smoothed particle hydrodynamics (SPH), readers are encouraged to consult the excellent recent review by Springel (2010b).

Using commercial CFD software could be an efficient way to perform computer simulations of astrophysical objects. However, this is usually not a viable solution because the requirements set by physical conditions in galaxies or star-forming clouds are extreme and very specific. Astrophysical flows are usually magnetized and strongly radiating, and, in most cases, they are self-gravitating. The model equations are therefore far from strict hyperbolic conservation laws, as is the case for traditional ideal fluids, but they feature complex source terms that drive the fluid conditions toward highly compressible, supersonic, and highly reactive conditions under which most traditional CFD codes miserably break.

In this review, I present the model equations that are used in (most) numerical hydrodynamics problems, from the ideal hydrodynamics (HD) or Euler equations to the ideal magnetohydrodynamics (MHD) equations to the radiation hydrodynamics (RHD) equations. I discuss the inclusion of nonideal terms, which model, usually very approximately, the deviation from local thermodynamical equilibrium (LTE). These terms are important to estimate the validity range of the HD equations, which usually break down for ultrararefied gases. Nonideal effects must then be included, introducing new numerical challenges. I then present the various source terms that are modeled in most astrophysical flows, such as, of course, gravity but also cooling and heating terms, centrifugal terms, etc. These source terms are the source of most numerical problems encountered by experts and are totally specific to astrophysics fluid flows. Numerical techniques developed in this context are discussed. Finally, I address more technical issues, such as increased numerical accuracy using optimal mesh strategies, as well as the available software packages to perform cutting-edge astrophysical fluid flows simulations.

2. MODEL EQUATIONS

2.1. Hydrodynamics Equations in Lagrangian Form

The simplest way to introduce the HD equations in the ideal limit is to start with the equations in Lagrangian form, following an infinitesimally small fluid element as it moves in space-time. The

volume of the fluid element is V; its mass, which is strictly conserved, is M; and the density, which evolves as the fluid elements deforms, is just

$$\rho = \frac{M}{V}. \tag{1}$$

The fundamental law of dynamics can be written for the fluid element using the Lagrangian time derivative as

$$\rho \frac{D\mathbf{u}}{Dt} = -\nabla P, \tag{2}$$

where we introduce two fundamental quantities for any fluid flow, namely the gas velocity vector $\mathbf{u}$ and the gas pressure P. The last missing equation comes from the first principle of thermodynamics and describes the evolution of the gas internal energy:

$$M \frac{D\epsilon}{Dt} = -P \frac{DV}{Dt}, \tag{3}$$

where ϵ is the specific internal energy (or the internal energy per unit mass).

Making use of the fact that the mass of the fluid element is strictly conserved,

$$\frac{DM}{Dt} = 0, \tag{4}$$

and we use the velocity divergence to measure the rate of change of the fluid volume V as

$$\frac{1}{V} \frac{DV}{Dt} = \nabla \cdot \mathbf{u} \tag{5}$$

to derive the HD equations in Lagrangian form:

$$\frac{1}{\rho} \frac{D\rho}{Dt} = -\nabla \cdot \mathbf{u}, \tag{6}$$

$$\rho \frac{D\mathbf{u}}{Dt} = -\nabla P, \tag{7}$$

and

$$\rho \frac{D\epsilon}{Dt} = -P \nabla \cdot \mathbf{u}. \tag{8}$$

We see that if we know the initial conditions of the flow, and if we know the fluid equation of state (EOS), which gives the thermal pressure as a function of density and internal energy,

$$P = P(\rho, \epsilon), \tag{9}$$

then the previous system of differential equations can be solved, at least numerically, for each fluid element describing the fluid.

The Lagrangian form of the Euler equations turns out to be very simple and can be used to design Lagrangian codes. These types of codes are very simple in one space dimension (1D), because one just needs to discretize the system of interest using mesh points regularly or irregularly spaced and then move these points in space-time using the Lagrangian derivative of the points' coordinates

$$\frac{D\mathbf{x}_i}{Dt} = \mathbf{u}(\mathbf{x}_i). \tag{10}$$

The index i stems from the mesh point number i, properly ordered, depending on the adopted geometry. Examples of such numerical implementations in 1D are given by Colella & Woodward (1984) and more recently by Murphy & Burrows (2008) and Commercon et al. (2011a) among many others. The SPH method is a particle-based technique that uses the Euler equation in Lagrangian form. Grid-based techniques with deformable Lagrangian meshes have also been

developed (Gnedin 1995, Pen 1997), but the mesh deformation usually becomes so extreme that large numerical errors can build up. However, a very elegant solution to this problem was found recently by Springel (2010a). We come back to this point at the end of the review.

There is another fundamental issue with the Euler equations in nonconservative, Lagrangian form: They are only valid far from discontinuities, and discontinuous solutions (shocks, contact discontinuity, vortex lines, triple points. . .) are common features in gas dynamics. It is therefore more convenient, both numerically and theoretically, to consider the Euler equations in their conservative and Eulerian form.

2.2. Hydrodynamics Equations in Eulerian Form

We use Reynolds's transport theorem to relate the Lagrangian time derivative of any scale quantity to its time and space partial derivatives

$$\frac{D(\cdot)}{Dt} = \frac{\partial(\cdot)}{\partial t} + \mathbf{u} \cdot \nabla(\cdot). \tag{11}$$

After a few standard manipulations, we obtain the Euler equation in Eulerian form as

$$\frac{\partial \rho}{\partial t} + \nabla \cdot (\rho \mathbf{u}) = 0, \tag{12}$$

$$\frac{\partial \rho \mathbf{u}}{\partial t} + \nabla \cdot (\rho \mathbf{u} \otimes \mathbf{u} + P\mathbb{I}) = 0, \tag{13}$$

and

$$\frac{\partial E}{\partial t} + \nabla \cdot [\mathbf{u}(E + P)] = 0, \tag{14}$$

in which we have introduced a new quantity, the fluid total energy per unit volume,

$$E = \rho\epsilon + \frac{1}{2}\rho \mathbf{u} \cdot \mathbf{u}. \tag{15}$$

The very important property of the Euler equations in this form is that they are in conservative form. They are just mere conservation laws, so that if one discretizes the computational volume into fixed volume elements, the time variations of the conserved quantities (mass, linear momentum, and total energy) are obtained by summing up the net fluxes through the computational cell faces. The flow variables can now be discontinuous; only the flux functions, which appear in the divergence operator, are required to be continuous through cell faces.

2.3. Godunov Method for Hyperbolic Systems of Conservation Laws

The previous set of equations is actually quite general in the sense that any system of conservation laws can be discretized following a similar strategy. One key additional property of the previous system is its hyperbolic nature. The easiest way to outline its importance is to linearize the previous system using the primitive variables (ρ, $\mathbf{u}$, and P). For the sake of simplicity, we assume that we have an ideal gas for which the EOS is simply $P = (\gamma - 1)\rho\epsilon$, where γ is the fluid adiabatic index. The previous conservative form can be modified into the so-called quasi-linear form:

$$\frac{\partial \rho}{\partial t} + \mathbf{u} \cdot \nabla \rho + \rho \nabla \cdot \mathbf{u} = 0, \tag{16}$$

$$\frac{\partial \mathbf{u}}{\partial t} + \mathbf{u} \cdot \nabla \mathbf{u} + \frac{1}{\rho}\nabla P = 0, \tag{17}$$

$$\frac{\partial P}{\partial t} + \mathbf{u} \cdot \nabla P + \gamma P \nabla \cdot \mathbf{u} = 0. \tag{18}$$

Although these equations are not valid close to a discontinuity, they are useful to perform a straightforward linearization of the Euler equations, leading to the dispersion relation of propagating sound waves,

$$c_s^2 = \frac{\gamma P}{\rho}. \tag{19}$$

If we are dealing with a set of conservation laws featuring propagating waves, the most popular numerical technique to solve the corresponding partial differential equations is the Godunov method (Godunov 1959, Toro 1999).

The numerical solution is obtained through the cell-averaged conservative variables $\mathbf{U}(\mathbf{x}, t) = (\rho, \rho\mathbf{u}, E)$:

$$\mathbf{U}_i^n = \frac{1}{V_i}\int_{V_i} \mathbf{U}(\mathbf{x}, t^n)\mathrm{d}V, \tag{20}$$

where the index i stands for the cell ordering (and its volume V_i) and index n stands for the discrete time coordinates. Using the divergence theorem, an exact integral form for the underlying set of conservation laws can be written as

$$\frac{\mathbf{U}_i^{n+1} - \mathbf{U}_i^n}{\Delta t} + \frac{1}{V_i}\int_{S_i} \bar{\mathbf{F}} \cdot \mathbf{n}\mathrm{d}S = 0, \tag{21}$$

where the time-averaged flux function is defined as

$$\overline{\mathbf{F}} = \frac{1}{\Delta t}\int_{t^n}^{t^{n+1}} \mathbf{F}(\mathbf{x}, t)\mathrm{d}t. \tag{22}$$

This methodology can be used to design numerical schemes at any order of accuracy and for any mesh geometry (Harten et al. 1983). We restrict ourselves to the Cartesian mesh geometry, because it allows exact cancellation of terms in the Taylor expansion and allows the corresponding numerical schemes to be of higher order than on irregular meshes (Calhoun & LeVeque 2000). We return to this point later in Section 7.

The traditional first-order Godunov technique considers that the numerical solution is piecewise constant in each cell, so that the cell average is equal to the solution everywhere in the cell. This is not true for higher-order Godunov methods, for which the solution is piecewise linear or piecewise parabolic inside each cell. The difficulty with the Godunov method lies in the numerical, time-averaged flux function. For the first-order method, because the solution is piecewise constant, we can define at each cell interface a so-called Riemann problem in which the solution is known exactly. The Riemann solution is self-similar in the variable x/t, i.e., in the direction normal to the interface. This allows a straightforward calculation of the flux function, because its time average is equal to its initial value at $x/t = 0$. This greatly simplifies the problem, and the flux function can be formally written as

$$\mathbf{F} = \mathbf{F}(\mathbf{U}_L, \mathbf{U}_R), \tag{23}$$

which is the Riemann solution for the input left and right piecewise constant states at $x/t = 0$.

In practice, the exact Riemann solution is never used, because it is too computationally expensive, and various approximate Riemann solvers are available for designing robust numerical schemes. The excellent book by Toro (1999) gives a complete accounting of the possible choices for Riemann solvers. For the sake of simplicity, we use here the simplest approximate Riemann solver know as the Lax-Friedrich flux function (LeVeque 1992), for which we have

$$\mathbf{F}(\mathbf{U}_L, \mathbf{U}_R) = \frac{\mathbf{F}_R + \mathbf{F}_L}{2} - \frac{S_{\max}}{2}(\mathbf{U}_R - \mathbf{U}_L). \tag{24}$$

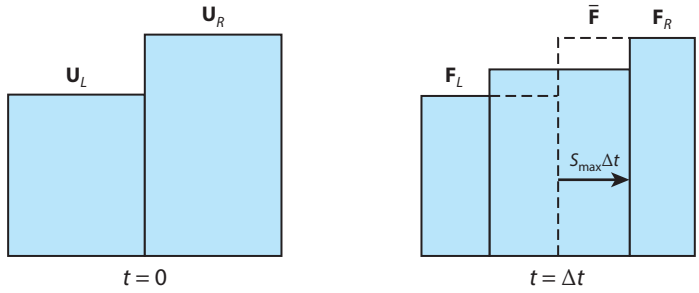

Figure 1

Schematics of the one-dimensional Riemann problem used to compute the intercell flux in the Godunov method.

This formula can be depicted as a classic Riemann problem as shown in **Figure 1**. This form is interesting because it features most of the important properties of the numerical solution of the HD equations. The first term, equal to the average of the left and right fluxes, is a second-order accurate approximation of the flux at the interface between the two cells. Using this term alone would result in a catastrophically unstable numerical solution. The second term stabilizes the numerical solution. This term is usually associated with numerical diffusion. It is indeed formally strictly equivalent to a flux proportional to the gradient of the conservative variable with a diffusion coefficient

$$\nu_{\text{num}} = \frac{S_{\max}\Delta x}{2}, \tag{25}$$

where Δx is the distance separating the two cells. The coefficient $S_{\max}$ encodes the maximum wave speed in the two cells. For the HD equation, $S_{\max}$ is given by

$$S_{\max} = \max\left[|\mathbf{u}\cdot\mathbf{n}|_L + (c_s)_L, |\mathbf{u}\cdot\mathbf{n}|_R + (c_s)_R\right]. \tag{26}$$

Stability is indeed ensured by "upwinding" the flux function with respect to the waves present in the solution. The Lax-Friedrich flux function can be considered overly conservative, because it upwinds the flux maximally with respect to all waves. It is therefore considered as maximally diffusive. Other approximate Riemann solvers are less diffusive while still being upwind with respect to each wave, which therefore minimizes numerical diffusion (Toro 1999).

It is very important to understand the following crucial points:

- Numerical diffusion is required to obtain a stable time integration.
- Numerical diffusion (for first-order schemes) is proportional to the cell size; therefore, it converges toward zero as the mesh size becomes infinitesimally small.
- For higher-order schemes, numerical diffusion can be significantly reduced, scaling with the cell size with a higher power, but it is still present to stabilize the numerical solution.
- It is often claimed in the literature that a numerical technique has "no advection error." Although this is true for strict Lagrangian schemes (modulo mesh-related issues), this is not always a desirable property, because the absence of numerical diffusion can promote various numerical instabilities together with poorly understood convergence properties.

Numerical diffusion is connected to a fundamental property of the HD equations: These are idealized equations, valid only in the LTE regime, in which one can neglect nonideal effects, such as viscosity and thermal conduction. The Euler equations are therefore obtained as the limit of the non-LTE HD equation with a vanishingly small viscosity and thermal conduction coefficients. Mathematically, the solution of the HD equations is therefore the solution of the nonideal equations with those nonideal terms converging to zero. One usually refers to this solution

as the weak solution of the HD equations—as opposed to the strong solution, which satisfies the HD equations with no viscous terms (Majda 1984). It is very important to understand that the only physically meaningful solution is the weak solution, because it is the one that comes from a realistic nonideal treatment of the underlying physics. It is also very important to realize that the numerical diffusion term we discussed above guarantees that the numerical solution is the weak solution, because the numerical problem we are solving comes with additional diffusive terms that mimic the nonideal terms.

In conclusion, we have learned that the Godunov scheme modified the underlying system of conservation laws, from a purely hyperbolic problem to a mixed hyperbolic and parabolic problem with a diffusion operator. A more detailed analysis is in general required to compute what is called the modified equation (ME) of the numerical scheme, usually by performing a Taylor expansion of the underlying finite difference approximation. In the present review, we have derived, using the Lax-Friedrich flux function, that the ME can be written as

$$\frac{\partial \mathbf{U}}{\partial t} + \nabla \cdot \mathbf{F}(\mathbf{U}) = \nu_{\text{num}} \Delta \mathbf{U}. \tag{27}$$

The right-hand side is our leading-order error term. It is also the reason why the scheme is stable and converges toward the weak solution of the Euler equations. This term can be reduced significantly using higher-order schemes (see Section 2.5). We have derived the exact value of the numerical diffusion coefficient for the Lax-Friedrich flux function. Note that if the numerical diffusion coefficient becomes negative, the underlying scheme is violently unstable. This can happen if the Riemann solver is not properly designed or if the mesh is very distorted (see next sections).

2.4. Nonideal Terms

To go beyond the ideal HD equations, one usually considers a microscopic description of the underlying gas particles. The classic approach is based on the Boltzmann equation, describing the evolution of the fluid through its distribution function and its collision integral (see, e.g., Mihalas & Mihalas 1984). If we assume that the flow conditions are close to LTE, the distribution function is quickly driven by collisions toward the Maxwellian distribution function, from which we can recover the ideal Euler equations presented above. Any deviation from LTE conditions perturbs the distribution function from the Maxwellian one. It can be shown that to first order, these deviations result in additional momentum and energy fluxes of the following form:

$$\frac{\partial \rho \mathbf{u}}{\partial t} + \nabla \cdot (\rho \mathbf{u} \otimes \mathbf{u} + P\mathbb{I}) = \nabla \cdot (\mu \mathbb{D}), \tag{28}$$

$$\frac{\partial E}{\partial t} + \nabla \cdot (\mathbf{u}(E + P)) = \nabla \cdot (\kappa \nabla T), \tag{29}$$

where $\mathbb{D}$ is the fluid deformation tensor, and μ is the dynamic viscosity coefficient, whereas κ is the conductivity coefficient, and T is the fluid temperature. Under normal conditions, μ and κ are very small but not strictly zero. These terms should always be considered at least formally in the physical solution of the HD equations. By contrast, when the gas becomes rarefied, these terms can dominate over the ideal ones, and the flow properties then deviate strongly from the ideal ones.

For a fully ionized, unmagnetized hydrogen plasma, one should use the Spitzer-Härm formulae (Spitzer & Härm 1953) for the proton dynamic viscosity and the electron thermal conductivity,

$$\mu_i \simeq 2 \times 10^{-15} \frac{T^{5/2}}{\ln \Lambda} \text{g cm}^{-1}\,\text{s}^{-1} \text{ and } \kappa_e \simeq 2 \times 10^{-5} \frac{T^{5/2}}{\ln \Lambda} \text{erg cm}^{-1}\,\text{s}^{-1}\,\text{K}^{-1}, \tag{30}$$

where the Coulomb logarithm, under average astrophysical conditions, is usually approximated using the ratio of the maximum to the minimum impact parameters (see, e.g., Mihalas & Mihalas 1984),

$$\Lambda = \frac{d_{\max}}{d_{\min}} \simeq 1.2 \times 10^4 \frac{T^{3/2}}{n^{1/2}}. \tag{31}$$

When the temperature falls below 10^5 K, the gas becomes neutral and Coulomb collisions are not relevant anymore. One should use collision between neutral hydrogen atoms (Joulain et al. 1998), leading to different viscosity and thermal conduction parameters,

$$\mu_n \simeq 10^{-4}\, T^{1/2}\,\mathrm{g\,cm^{-1}\,s^{-1}} \text{ and } \kappa_n \simeq 2 \times 10^4 T^{1/2}\,\mathrm{erg\,cm^{-1}\,s^{-1}\,K^{-1}}. \tag{32}$$

We can express these microscopic transport coefficients as diffusion coefficients using

$$\nu_{\mathrm{visc}} = \frac{\mu}{\rho} \quad \text{and} \quad \nu_{\mathrm{heat}} = \frac{\kappa}{\rho C_v}, \tag{33}$$

where C_v is the specific heat capacity at constant volume. We can estimate the relative importance of these two diffusive processes by computing the Prandtl number $\mathrm{P} = \nu_{\mathrm{visc}}/\nu_{\mathrm{heat}}$ as the ratio of the viscous one over the thermal one. For an ionized plasma, one finds $\mathrm{P} \simeq 0.01$, illustrating the dominance of electronic thermal conduction over ionic viscosity (Balbus & Henri 2008). It is worth mentioning that, using the Lax-Friedrich flux function, one finds a numerical Prandtl number equal to one, because the diffusion coefficients for the momentum and the energy are the same.

To estimate the importance of these nonideal effects on the system of interest, one can also compute the viscous Reynolds number,

$$\mathrm{Re} = \frac{UL}{\nu_{\mathrm{visc}}}, \tag{34}$$

where U and L are typical velocity and length scales, respectively, in the system of interest. If $\mathrm{Re} \simeq 1$–100, then viscous effects are likely to dominate the flow, whereas for large Reynolds numbers, viscosity can be ignored and the flow is likely to become turbulent. Another important consideration is to compare the physical viscosity to the numerical diffusivity. Indeed, if $\nu_{\mathrm{num}} \simeq \nu_{\mathrm{visc}}$, then one can also ignore the physical viscosity, because the numerical viscosity associated to the Godunov scheme dominates. It is possible to define a numerical Reynolds number as

$$\mathrm{Re}_{\mathrm{num}} = \frac{UL}{\nu_{\mathrm{num}}} \simeq \frac{2L}{\Delta x}, \tag{35}$$

where we used for the maximum wave speed $S_{\max} = U$ for our first-order Godunov scheme. However, the numerical viscosity does not behave exactly as the physical one. It is therefore legitimate to model the underlying system, including both viscosity and thermal conduction, to make sure that the underlying numerical scheme converges to the same solution. For higher-order Godunov schemes, numerical diffusion can be reduced significantly, but its functional form deviates also more strongly from the underlying physical diffusion processes. It is therefore of primary importance to validate the overall methodology, by performing small-scale simulations in which physical diffusion processes are resolved and modeled as additional source terms (see, for example, Fromang et al. 2007).

2.5. Higher-Order Schemes

Although the first-order Godunov scheme features nice properties, such as a controlled numerical diffusivity, which ensures the proper numerical convergence toward the weak solution of the

underlying set of conservation laws, the numerical diffusion is usually too large for practical applications. The leading-order error terms are indeed quite large, and they are proportional to the grid spacing, making the convergence toward the exact solution quite slow. This has led to the development of higher-order schemes, the first of its kind being the second-order scheme of van Leer, the so-called MUSCL scheme (van Leer 1976). Second-order schemes are based on a piecewise linear representation of the solution inside each cell. In 3D, it means we have to determine three additional coefficients per variable describing the slope of the affine function:

$$w(\mathbf{x}) = w(\mathbf{x}_i) + \nabla \mathbf{w}_i \cdot (\mathbf{x} - \mathbf{x}_i), \tag{36}$$

where the vector $\nabla \mathbf{w} = [(\Delta w)_x, (\Delta w)_y, (\Delta w)_z]$ encodes the local gradient of the primitive variables $w = \rho$, u_x, u_y, u_z, or P; and $\mathbf{x}_i$ is the cell center, cell center of mass, or cell centroid, depending on the adopted mesh geometry. One can also use an even higher-order polynomial representation of the solution, in which one has

$$w(\mathbf{x}) = w(\mathbf{x}_i) + \sum_{a,b,c}^{a+b+c \le q} (\Delta w)_{a,b,c} (x - x_i)^a (y - y_i)^b (z - z_i)^c, \tag{37}$$

where q is the order of the polynomial form. Starting from this spatial representation of the numerical solution, we can use two different paths to design high-order numerical schemes. The first class of techniques could be referred to as finite element schemes (Zienkiewicz & Morice 1971) or discontinuous Galerkin methods (Cockburn & Shu 1998). The idea is that the four (or more) high-order coefficients used to describe one variable are four-or-more degrees of freedom for which we need to solve their time evolution. We thus move from five variables (our cell-averaged states) to $5 \times 4 = 20$ (or more) coefficients to be updated at each time step. This finite element or discontinuous Galerkin approach is very compact in the sense that one can derive the time evolution equations for each of the polynomial coefficients using only one neighboring cell in each direction. The storage requirements are quite massive, however. The second class of techniques is usually referred to as finite-volume methods or essentially non-oscillatory (ENO) schemes (Shu & Osher 1988). In this second approach, the degrees of freedom are just the five cell-averaged conservative variables. The coefficients of the polynomial representation are computed at each time step using $q + 1$ neighboring cells, within the so-called stencil. These are just intermediate variables that are discarded at the end of the time step. The main drawback of the ENO method is, therefore, its relatively nonlocal nature.

The main complexity of high-order schemes arises when one needs to perform spatial and temporal quadratures to compute the flux through cell faces. Because the solution is not piecewise constant but piecewise linear, parabolic, or more, the Riemann problems at the cell interface are not self-similar anymore. One should therefore estimate the solution at several quadrature points in time and space to perform the time and face averages of the fluxes. Several techniques have been developed to address this issue: predictor-corrector strategies, Runge-Kutta schemes, high-order Taylor expansions (see, among others, Suresh & Huynh 1997, Titarev & Toro 2002). They all have drawbacks and advantages and are significantly more complex in 2D and 3D than in 1D.

Another area of research and development in the design of high-order ENO schemes is precisely the computation of the polynomial coefficients. It is indeed well known that high-order polynomial reconstruction tends to be oscillatory and exhibits difficulties in preserving the positivity of the solution. For second-order schemes, one uses traditionally slope limiters to ensure the positivity

and the smoothness of the solution. Slope limiters are nonlinear functions of the existing solution that automatically detect strong discontinuities and extrema in the solution variables, preventing the formation of additional spurious features in the computed solution (Hubbard 1999). For more than third-order schemes, the situation is much more complicated, and several strategies have been developed in the context of the ENO approach to minimize these spurious effects (see, for example, Jiang & Wu 1999). This component of high-order schemes is probably the most important one, needing the design of robust numerical schemes that can sustain the extreme requirements of the highly compressible astrophysical flows.

High-order methods are usually very efficient to capture smooth features of the flow, such as large vortices, smooth interfaces, or slowly varying density and velocity profiles. As a result of the highly compressible nature of astrophysical fluid flows, however, it is quite common to find many interacting discontinuities with severe singularities; for such cases, high-order schemes are less efficient than low-order schemes used at a much higher mesh resolution. Adaptive meshes allow refinement of the grid adaptively, so that discontinuities are better captured even with a low-order scheme. This probably explains why very high-order schemes (with $q > 2$) were never really used for production runs in astrophysics. However, in recent years several new codes have been developed with more third- and fourth-order accuracy with relatively cheap algorithms (McCorquodale & Colella 2011, Woodward et al. 2013, Boscheri & Dumbser 2014 and references therein). Very high-order schemes become more popular in the astrophysical community, which may improve significantly the quality of the simulations. Coupled to adaptive mesh and moving mesh (MvM) strategies, we may be able to design the new generation of astrophysical codes to feature both high resolution and high accuracy.

3. MAGNETOHYDRODYNAMICS

3.1. Ideal Magnetohydrodynamics Equations

In a magnetized fluid, the HD equations need to be modified to account for the Lorentz force. In Lagrangian form, the only modification arises in the fluid acceleration, which now reads as

$$\rho \frac{D\mathbf{u}}{Dt} = -\nabla P + \mathbf{J} \times \mathbf{B}, \tag{38}$$

where $\mathbf{B}$ is the magnetic field and $\mathbf{J}$ is the current, defined in the so-called MHD limit by

$$\mathbf{J} = \nabla \times \mathbf{B}. \tag{39}$$

The fluid equations have to be supplemented by the induction equation, which reads, in the so-called ideal MHD limit,

$$\frac{\partial \mathbf{B}}{\partial t} = -\nabla \times \mathbf{E}, \tag{40}$$

where the electric field is $\mathbf{E} = -\mathbf{u} \times \mathbf{B}$, and the magnetic field satisfies the divergence free constraint $\nabla \cdot \mathbf{B} = 0$. The ideal MHD limit is reached when one can neglect Ohmic dissipation and ambipolar diffusion terms, as well as viscosity and thermal conduction, like for the ideal Euler equations.

After a few classic derivations, the ideal MHD equations in their conservative, Eulerian form can be derived as

$$\frac{\partial \rho}{\partial t} + \nabla \cdot (\rho \mathbf{u}) = 0, \tag{41}$$

$$\frac{\partial \rho \mathbf{u}}{\partial t} + \nabla \cdot (\rho \mathbf{u} \otimes \mathbf{u} - \mathbf{B} \otimes \mathbf{B} + P_{\rm tot} \mathbb{I}) = 0, \tag{42}$$

and

$$\frac{\partial E_{\rm tot}}{\partial t} + \nabla \cdot [\mathbf{u}(E_{\rm tot} + P_{\rm tot}) - \mathbf{B}\,(\mathbf{B} \cdot \mathbf{u})] = 0, \tag{43}$$

where we have introduced two new quantities, the fluid total energy per unit volume,

$$E_{\rm tot} = \rho\epsilon + \frac{1}{2}\rho \mathbf{u} \cdot \mathbf{u} + \frac{1}{2}\mathbf{B} \cdot \mathbf{B}, \tag{44}$$

and the total pressure,

$$P_{\rm tot} = P(\rho, \epsilon) + \frac{1}{2}\mathbf{B} \cdot \mathbf{B}. \tag{45}$$

This set of partial differential equations is also a hyperbolic system of conservation laws, to which the Godunov methodology directly applies. One can also derive a quasi-linear form of the previous system and compute the properties of the various waves present in the flow. The most important new wave is the Alfvén wave, for which the wave speed is given by

$$c_{\rm A}^2 = \frac{B^2}{\rho}. \tag{46}$$

Two more new waves are present, which are modifications of the classic sound waves of the HD equations, the fast and slow magnetosonic waves. Because the wave pattern of the MHD equations is significantly richer than the HD case, the MHD Riemann solvers are more complicated. The Lax-Friedrich approximate Riemann solver is still very simple, with the maximum wave speed chosen to be the fast magnetosonic speed. Other Riemann solvers have been designed for MHD, such as the Roe MHD linear solver (Cargo & Gallice 1997) or the HLLD (Harten-Lax-van Leer with discontinuities) MHD nonlinear solver (Miyoshi & Kusano 2005). The latter approximate Riemann solver has been probably the most popular one for the past few years (Fromang et al. 2006, Stone et al. 2008, Balsara et al. 2014, Kim & Balsara 2014).

The real challenge in designing a numerical scheme for the MHD equations lies in the numerical representation of the magnetic field and how one solves the induction equation. There are two possible strategies: The first one follows from the obvious simplifying choice that the magnetic field is also defined as a volume average of the underlying 3D magnetic field within the volume of each cell:

$$\mathbf{B}_i^n = \frac{1}{V_i} \int_{V_i} \mathbf{B}(\mathbf{x}, t^n) \mathrm{d}V\,. \tag{47}$$

In this way, the magnetic field variable is treated on exactly the same footing as the other HD variables (ρ, $\mathbf{u}$, and P). However, two new problems appear: First, one must transform the induction equation, which, from Stokes' theorem, is more naturally discretized using the circulation of the electric field around a surface element into an integral form using the flux of the electric field around a volume element. The second problem is related to the divergence free constraint (Tóth 2000). The resulting numerical approximation of the magnetic field does not necessarily satisfy $\nabla \cdot \mathbf{B} = 0$ at each intermediate step in the algorithm. This introduces small spurious magnetic monopoles, which affect the jump conditions of MHD shock waves and can result in severe instabilities in the

flow. The traditional solution to this potentially dramatic problem is to use divergence cleaning techniques. The first proposed solution was to explicitly remove the divergence from the flow, solving a Poisson equation and removing the gradient of the solution to the magnetic field:

$$\Delta\phi = \nabla \cdot \mathbf{B}^{\rm old} \quad \text{and} \quad \mathbf{B}^{\rm new} = \mathbf{B}^{\rm old} - \nabla\phi. \tag{48}$$

This divergence cleaning operator guarantees by construction that the magnetic field remains divergence free (Brackbill & Barnes 1980). However, it is not an ideal solution for several reasons: First, magnetic monopoles still appear in the flow, and affect it in a nonlocal way, owing to the Laplacian operator; second, solving the Poisson equation is quite time consuming; and third, for high-order schemes, predictor-corrector or Runge-Kutta strategies require multiple updates of the magnetic field with, in principle, multiple divergence cleaning steps needed (Crockett et al. 2005). A popular alternative is Powell's eight-wave scheme, which directly accounts for the presence of magnetic monopoles in the numerical scheme (Powell et al. 1999). The scheme is therefore not strictly conservative for the magnetic flux, leading to small violations of the underlying conservation laws. In the case of strong shocks, this can be problematic. Magnetic monopoles are advected in the flow and, thanks to the numerical diffusion of the underlying advection scheme, damped out with the flow. However, note that this strategy, though very cheap and quite accurate in the case of high-order MHD schemes, can under some circumstances fail dramatically: This occurs in the presence of the stagnation point, in which magnetic monopoles can accumulate, like in the Great Pacific garbage patch. Additional damping can be enforced close to stagnation points using extra divergence cleaning (Dedner et al. 2002). A last note of caution: Recently developed MvM codes have been designed to minimize very significantly the numerical diffusion associated with pure advective flows, as compared with classical Eulerian schemes. Used with Powell's eight-wave scheme, this could potentially lead to the formation of strong, long-lived magnetic monopoles, precisely because the only damping process of the magnetic monopoles, namely numerical diffusion, has been removed (Tóth 2000, Pakmor & Springel 2013). Fortunately, a much more robust approach, the so-called constrained transport technique, has been recently implemented for MvM MHD codes (Mocz et al. 2014).

Constrained transport is actually the second viable strategy for solving the induction equation (Evans & Hawley 1988). It is based on a more complicated discretization of the flow variables, with the HD variables (ρ, $\mathbf{u}$, and P) still defined as cell-averaged quantities, whereas the magnetic field is defined as a surface-averaged quantity, normal to the interfaces of each cell, precisely where the flux function is defined:

$$B^n_{\rm face} = \frac{1}{S_{\rm face}} \int_{S_{\rm face}} \mathbf{B}(\mathbf{x}, t^n) \cdot \mathbf{n}\, {\rm d}S. \tag{49}$$

In this framework, one must define one magnetic field component per face. For a simple Cartesian geometry, neighboring cells share the same faces, and the overall memory footprint of this so-called staggered mesh approach is exactly the same as the fully cell-centered approach. For more complex mesh geometries, this could result in a significant overhead, depending on how many more faces one must deal with. The great advantage of this approach is the straightforward derivation of an integral form of the induction equation, using Stokes' theorem directly on each face of the computational cells:

$$\frac{\partial \mathbf{B}}{\partial t} \cdot {\rm n} = \frac{B^{n+1}_{\rm face} - B^n_{\rm face}}{\Delta t} = -\frac{1}{S_{\rm face}} \int_{L_{\rm face}} \mathbf{E} \cdot {\rm d}\ell, \tag{50}$$

where the integral is taken over the contour surrounding the surface element. The immediate gain of the constrained transport technique is that the magnetic flux through the ensemble of faces defining each computational cell is automatically conserved. Indeed, because two neighboring

faces are sharing the same line contour element but are oriented in opposite directions, the line integrals cancel exactly, leading to the relation

$$\sum_{\text{face}} B^{n+1}_{\text{face}} S_{\text{face}} = \sum_{\text{face}} B^{n}_{\text{face}} S_{\text{face}}. \tag{51}$$

If initially the magnetic field is divergence free, then the sum over the faces vanishes exactly, and the previous relation ensures that the sum over the faces remains zero during the entire evolution. The constrained transport scheme was used in the finite difference code, ZEUS (Stone & Norman 1992), and was only rather recently adapted to the Godunov methodology (Londrillo & del Zanna 2004, Fromang et al. 2006). This very powerful method creates two major complications: First, it is mandatory for the initial magnetic field to satisfy the divergence free condition exactly. This usually requires a careful initialization of the field, traditionally using the curl of the potential vector $\mathbf{B} = \nabla \times \mathbf{A}$. Second, we must compute the electric field on the line segments running around each face. For the resulting scheme to be stable, proper unwinding of the electric field is required using the HD variables from the neighboring cells and the magnetic field from the neighboring faces. For a Cartesian mesh geometry, each edge is surrounded by four cells and four faces. Therefore, we must deal with a two-dimensional Riemann problem with four quadrants defining four piecewise constant MHD states. This is a major complication compared with traditional cell-centered schemes on Cartesian meshes, which have only one-dimensional Riemann problems that are solved perpendicular to each interface. Hopefully, many approximate two-dimensional Riemann solvers have been developed in recent years, making the constrained-transport method a viable solution for Godunov schemes (Londrillo & del Zanna 2004, Fromang et al. 2006, Balsara et al. 2014). It is also worth mentioning that fully cell-centered schemes that are based on one-dimensional Riemann solvers are truly second-order schemes for Cartesian meshes only in which exact cancellation of high-order transverse terms in the Taylor expansion is performed thanks to symmetries of the mesh. For arbitrarily shaped, unstructured meshes, second-order accuracy is not maintained anymore if one uses only one-dimensional Riemann solvers perpendicular to the cell faces. To restore second-order accuracy for unstructured meshes, one should again rely on multidimensional Riemann solvers defined on the nodes (Balsara et al. 2014, Vilar et al. 2014).

The simplest two-dimensional Riemann solver is here again the Lax-Friedrich MHD Riemann solver (Londrillo & del Zanna 2004), which has, for the electric field component in the z-direction, $E_z = u_y B_x - u_x B_y$, located on cell edges pointing in the z-direction, as

$$E_z = \frac{(E_z)_{LB} + (E_z)_{LT} + (E_z)_{RB} + (E_z)_{RT}}{4}, \tag{52}$$

$$- \frac{(S_y)_{\max}}{2} \left[(B_x)_T - (B_x)_B\right], \tag{53}$$

and

$$+ \frac{(S_x)_{\max}}{2} \left[(B_y)_R - (B_y)_L\right]. \tag{54}$$

This formula can be understood as the solution of a two-dimensional Riemann problem, as shown in **Figure 2**. A very interesting consequence of the two-dimensional unwinding procedure is that the numerical electric field is here also decomposed into two terms: the first one being the accurate, but potentially unstable, average of the electric field in the four quadrants and the second term being the stabilizing term, which has the exact same mathematical form as a magnetic diffusivity, with a magnetic numerical diffusion coefficient equal to its HD counterpart. Therefore, we end up with a numerical approximation of the ideal MHD equations that features a proper magnetic

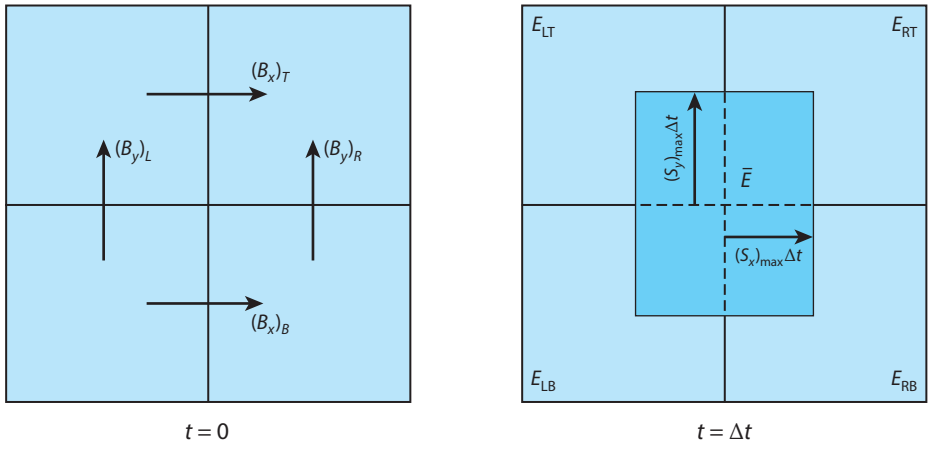

Figure 2

Schematics of the two-dimensional Riemann problem used to compute the electric field at cell edges in the magnetohydrodynamics Godunov scheme.

diffusion term, allowing magnetic reconnection to occur in a physically motivated way and recovery of the weak solution of the ideal MHD equations.

3.2. Nonideal Magnetohydrodynamics

Another interesting consequence of this nice important property is the fact that numerical diffusion for the magnetic field behaves in a fashion similar to numerical diffusion for the hydro variable. If one is interested in nonideal MHD effects, in which physical diffusion processes are now considered, namely fluid viscosity and magnetic resistivity, one must define a new number related to magnetic diffusivity, called the magnetic Reynolds number:

$$\mathrm{Re_M} = \frac{UL}{\nu_\mathrm{M}}. \tag{55}$$

To assess the relative roles of viscosity and resistivity, we can also introduce the magnetic Prandtl number, which is the ratio of the viscous diffusivity to the magnetic one (see, e.g., Balbus & Henri 2008):

$$\mathrm{P_M} = \frac{\nu_\mathrm{visc}}{\nu_\mathrm{M}}. \tag{56}$$

From our analysis in the previous section, we conclude that Godunov schemes have also the property that the numerical magnetic Prandtl number can be $\mathrm{P_M} \simeq 1$, which can have significant consequences on the properties of the corresponding MHD flow, such as affecting the saturation properties of MHD turbulence. A definitive answer on the physics of MHD turbulence and MHD reconnection cannot be obtained without properly modeling nonideal effects (Fromang et al. 2007). The first microscopic effect to add to the previous ideal description is the Ohmic dissipation, which enters the electric field definition as

$$\mathbf{E} = -(\mathbf{u} \times \mathbf{B}) + \nu_\mathrm{M}\mathbf{J}. \tag{57}$$

For a fully ionized hydrogen plasma, the magnetic diffusivity can be computed using the Spitzer-Härm formula for Coulomb collisions,

$$\nu_{\rm M} \simeq 1.2 \times 10^{11} \frac{\ln \Lambda}{T^{3/2}} \, {\rm cm}^2 \, {\rm s}^{-1}, \tag{58}$$

and the corresponding magnetic Prandtl number takes the nontrivial form

$$\mathrm{P_M} \simeq 10^{-2} \frac{T^4}{n \left(\ln \Lambda\right)^2}, \tag{59}$$

which is much larger than one for most astrophysical applications, except for star-forming molecular core and protoplanetary discs, as well as compact objects, in which the hydrogen number density is larger than 10^{14} H cc^{-1}. Note that this density corresponds also to the regime in which the gas becomes opaque to its own radiation, and radiative effects need to be included, as we discuss in the next section. When the gas temperature is lower than 10^4 K, the gas becomes neutral or even molecular, and Coulomb collisions are not relevant anymore. Ohmic dissipation becomes much larger in this regime, ultimately infinite when the ionization fraction tends to zero, leading to the formation of dead zones. This regime is very challenging for numerical codes, because, as seen in the following sections, the nonideal effects dominate over the HD equations (see, for example, the recent work by Lesur et al. 2014).

When the gas becomes very weakly ionized, other nonideal effects must be incorporated in the MHD equations. The most famous one in the context of star formation is ambipolar diffusion (Shu 1992). When the number density of charged particles (electron and ions) becomes very small, neutral and molecular species are drifting away from the charged ones, and the MHD equations can be written in a more suitable form in which the fluid velocity is mostly given by neutral particles, but the magnetic field is frozen in the charge velocity. The drift velocity among ions and neutrals, $\mathbf{u}_{\rm d} = \mathbf{u}_{\rm i} - \mathbf{u}_{\rm n}$, is set to its equilibrium value, balancing the friction force with the Lorentz force,

$$\mathbf{u}_{\rm d} = \frac{\tau_{\rm in}}{\rho_{\rm i}} \mathbf{J} \times \mathbf{B}, \tag{60}$$

and acts as a diffusion process for the magnetic field lines. The friction is parameterized by the mean collision timescale between neutral and ionized species $\tau_{\rm in}$. The MHD equations remain unchanged, using for the velocity field $\mathbf{u} = \mathbf{u}_{\rm n}$, except for the induction equation that uses $\mathbf{u}_{\rm i} = \mathbf{u} + \mathbf{u}_{\rm d}$, so that $\mathbf{E} = -(\mathbf{u} \times \mathbf{B}) - (\mathbf{u}_{\rm d} \times \mathbf{B})$. The mathematical form of the ambipolar diffusion operator is very complicated. It can be very roughly interpreted as a classic diffusion operator with a highly nonlinear diffusion coefficient. One can approximate this diffusion coefficient as

$$\nu_{\rm AD} \simeq \tau_{\rm in} c_{\rm A}^2, \quad \text{where} \quad \tau_{\rm in} \simeq \frac{10^{-13} \, {\rm g/cc}}{\rho x_{\rm i}} {\rm s} \tag{61}$$

and $x_{\rm i}$ is the ionization fraction. In order for this new nonideal effect to be relevant, we can form the ambipolar diffusion (AD) Reynolds number for the system under study, and we also must compare this coefficient to the numerical diffusion coefficient, which, in the case of a strong magnetic field, is just

$$\nu_{\rm num} \simeq \frac{c_{\rm A} \Delta x}{2}. \tag{62}$$

If the numerical diffusion coefficient dominates, then including AD is not necessary. In contrast, if the AD diffusion coefficient dominates, it affects the dynamics. If this coefficient becomes very large, then we enter another regime in which this additional nonideal term becomes stiff with respect to the MHD equations (see Section 6).

4. RADIATION HYDRODYNAMICS

Radiation processes are very important in astrophysical fluid dynamics. Microscopic collisions drive the particle distribution function toward the Maxwellian form and justify our fluid approach, namely the MHD equations with the potential addition of small, nonideal source terms. But these very collisions also excite atoms and molecules and trigger the emission of radiation. Only under very dilute conditions (in the hot, low-density plasma in galaxy clusters, for example) can we ignore these radiation losses, but in practice, this is never the case in galaxy and star-formation simulations. On large scales, radiation can be treated as optically thin, and we can model it as a pure gas energy sink term. However, on small scales radiation becomes optically thick, and we need to model how radiation is transported through the fluid and how it interacts dynamically and energetically with it. We now describe the realm of RHD.

4.1. The Equation of Radiative Transfer

The main equation we have to solve is the radiative transfer (RT) equation, which is discussed in any introductory courses in astronomy and astrophysics (see, for example, Rybicki & Lightman 2008). In the present context, it is worth mentioning that the RT equation is nothing else than the Boltzmann equation for photons, which are a rather peculiar and simple fluid because they flow at a constant speed, namely the speed of light. Photon momentum is not described by three velocity components but by two Euler angles and one energy $E = h\nu$ component in which ν is the radiation frequency. The Boltzmann equation for radiation takes the following form:

$$\frac{1}{c}\frac{\partial I_\nu}{\partial t} + \mathbf{n}\frac{\partial I_\nu}{\partial \mathbf{x}} = -\kappa_\nu I_\nu + \eta_\nu, \tag{63}$$

where κ_ν and η_ν are, respectively, the absorption and emission coefficients. The equation depends on seven independent variables: one of time, three of space, two angles defining the direction of propagation of photons, and finally the photon energy. Exactly as for the usual Boltzmann equation, it is customary to take moments of the radiation intensity, I_ν, by integrating over all possible directions for a given solid angle, $\mathrm{d}\Omega$. We can then define the first three moments of the radiation field as (Mihalas & Mihalas 1984)

$$E_\nu(\mathbf{x}, t) = \int_{4\pi} I_\nu(\mathbf{x}, \mathbf{n}, t)\frac{\mathrm{d}\Omega}{c} : \text{radiation energy density}, \tag{64}$$

$$\mathbf{F}_\nu(\mathbf{x}, t) = \int_{4\pi} I_\nu(\mathbf{x}, \mathbf{n}, t)\mathbf{n}\mathrm{d}\Omega : \text{radiation flux vector}, \tag{65}$$

and

$$\mathbb{P}_\nu(\mathbf{x}, t) = \int_{4\pi} I_\nu(\mathbf{x}, \mathbf{n}, t)\mathbf{n}\otimes\mathbf{n}\frac{\mathrm{d}\Omega}{c} : \text{radiation pressure tensor}. \tag{66}$$

Using these definitions and integrating the RT equation over the angles, we obtain a set of two conservation laws that are very similar to the Euler equations. These are called the radiation moment equations:

$$\frac{\partial E_\nu}{\partial t} + \nabla\cdot\mathbf{F}_\nu = -\kappa_\nu c\, E_\nu + S_\nu : \text{conservation of energy} \tag{67}$$

and

$$\frac{\partial \mathbf{F}_\nu}{\partial t} + c^2\nabla\cdot\mathbb{P}_\nu = -\kappa_\nu c\mathbf{F}_\nu : \text{conservation of momentum}, \tag{68}$$

where the total plasma emissivity is now described by the function

$$S_\nu = \int_{4\pi} \eta_\nu \mathrm{d}\Omega. \tag{69}$$

The previous set of equations is unfortunately not closed, because we need to know the value of the pressure tensor to be able to solve for the radiation flux. We rely on various numerical techniques and approximation to model this pressure tensor. It is worth mentioning that the computational power of present-day supercomputers allows one to directly solve the RT equation in phase space. We need to discretize the angular domain and the frequency domain, for which solving the RT equation becomes a trivial advection problem with a constant speed, $\mathbf{u} = c\,\mathbf{n}$. When the corresponding flow is relativistic, the time step requirement for a stable explicit integration is moreover the same as the HD solver, so that the coupled RT-HD problem becomes tractable in its full glory (Jiang et al. 2014).

4.2. Coupling Radiation to Hydrodynamics

To evaluate the effect of radiation on the dynamics of the gas, we must couple the RT equation to the Euler equations. This is done through interaction processes between photons and particles in the flow. For each photon absorbed or emitted, there is a corresponding exchange of momentum and energy between the fluid and the radiation. We have already seen the corresponding source and sink terms in the radiation momentum and energy equations. We need to compute now the corresponding source and sink of momentum and energy for the gas. The energy equation, written here for the total fluid energy $E = \rho\epsilon + \frac{1}{2}\rho u^2$, must be modified to

$$\frac{\partial E}{\partial t} + \nabla \cdot [\mathbf{u}(E + P)] = \Gamma_{\mathrm{rad}} - \Lambda_{\mathrm{rad}}. \tag{70}$$

The source term Γ is called the heating function, whereas the sink term Λ is called the cooling function. They are computed by integrating over the photon frequencies the absorbed radiation energy and the emitted radiation energy:

$$\Gamma_{\mathrm{rad}} = \int_0^{+\infty} \kappa_\nu c\, E_\nu \mathrm{d}\nu \quad \text{and} \quad \Lambda_{\mathrm{rad}} = \int_0^{+\infty} S_\nu \mathrm{d}\nu. \tag{71}$$

The momentum equation has only one source term and no sink term, because the emitted radiation field is always isotropic. It reads, in conservative form,

$$\frac{\partial \rho\mathbf{u}}{\partial t} + \nabla \cdot (\rho\mathbf{u} \otimes \mathbf{u} + P\mathbb{I}) = \mathbf{F}_{\mathrm{rad}}, \tag{72}$$

where the radiation force is just the momentum gained by absorbing the incident radiation,

$$\mathbf{F}_{\mathrm{rad}} = \int_0^{+\infty} \frac{\kappa_\nu}{c} \mathbf{F}_\nu \mathrm{d}\nu. \tag{73}$$

The critical ingredient in describing the coupled evolution of gas and radiation is the opacity κ_ν. This quantity is determined by the microphysics of the fluid under consideration. In galaxy formation, at high temperature, atomic physics determines the opacity of the fluid and the associated cooling and heating rates. Collisional processes, such as (photo- and collisional) ionizations, recombinations, and excitations, are responsible for most of the radiative losses. At lower temperature, around and below 1,000 K, fine-structure transitions of carbon and oxygen atoms become important. Below 1,000 K, H_2 and CO molecules form, in conjunction with and thanks to dust grains, bringing in new cooling processes. Radiation is very sensitive to these new chemical components, especially to the opacity of dust grains.

Note also that one needs to include relativistic corrections to the opacity owing to Doppler effects between the laboratory frame, in which the radiation variables are defined, and the comoving frame, in which microscopic interactions are taking place (Mihalas & Mihalas 1984). This leads to additional terms of order v/c that are omitted here for the sake of simplicity that could play a very important role, depending on the application. Variants of the previous RHD equations can also be derived, assuming that they are written entirely in the comoving frame or even in mixed frames (Lowrie et al. 1999, Krumholz et al. 2007).

4.3. Numerical Techniques for Radiation Hydrodynamics

We have seen that both the full RT equation (discretized in angular space) and the moment equations are relatively simple transport equations (ignoring the source terms) of hyperbolic nature. Here again, we can apply the Godunov methodology to solve these equations. For the moment equations, a very important ingredient is still missing: What form do we adopt for the radiation pressure tensor, $\mathbb{P}_\nu = E_\nu \mathbb{D}_\nu$, in which $\mathbb{D}_\nu$ is the Eddington tensor that encodes the geometry of the local radiation field (Mihalas & Mihalas 1984)?

Several numerical techniques have been designed to estimate the pressure tensor. The simplest technique is based on the diffusion approximation, in which case the pressure tensor is strictly isotropic. The radiation flux is then proportional to the gradient of the radiation energy. This has led to the implementation of the flux-limited diffusion (FLD) method, presented in the astrophysical context, for example, by Stone et al. (1992). This technique is still very popular today (Krumholz et al. 2007, Commercon et al. 2011b), although it suffers from well-known caveats, such as the lack of shading effect. The most elaborate numerical technique is probably the variable Eddington tensor (VET) approach (Jiang et al. 2012), in which one solves the time-independent RT equation, discretizing the angular domain. This is clearly the expensive part of the method, but the complex geometry of the resulting static radiation field allows one to estimate the Eddington tensor with great accuracy. A variant of this method has also been proposed earlier in the cosmological context, known as the optically thin VET or OTVET (Gnedin & Abel 2001), in which one solves the static full RT equation in empty space. Another interesting alternative to both FLD and VET has been proposed by Levermore (1984) and used in various recently developed RHD solvers (González et al. 2007, Aubert & Teyssier 2008, Skinner & Ostriker 2013); it is called the M1 approximation, in which the Eddington tensor is just a function of E_ν and $\mathbf{F}_\nu$:

$$\mathbb{D}_\nu = \frac{1-\chi_\nu}{2}\mathbb{I} + \frac{3\chi_\nu - 1}{2}\mathbf{n}_\nu \otimes \mathbf{n}_\nu, \tag{74}$$

with

$$\chi_\nu = \frac{3+4f_\nu^2}{5+2\sqrt{4-3f_\nu^2}} \quad \text{and} \quad \mathbf{f}_\nu = f_\nu \mathbf{n}_\nu = \frac{\mathbf{F}_\nu}{cE_\nu}. \tag{75}$$

This particular mathematical form comes from the assumption that the radiation field can be fitted locally by a simple dipole. One important consequence of this very crude approximation is that two equally strong sources can never be properly described by the M1 approximation. As soon as one moves close enough to a strong source, the approximation becomes more accurate. The other important consequence of the M1 approximation is that the resulting system of conservation laws is strictly hyperbolic: one can therefore treat radiation as a fluid, with traveling waves moving at or close to the speed of light. The Godunov methodology can therefore be applied in this context too. The typical wave speed is however very large, and special care must be taken to perform the time integration of the resulting equations.

In any case, once the Eddington tensor has been computed, one just solves the two moment equations using the Godunov methodology. The radiation moment variables are defined as cell-centered, volume-averaged quantities, and both the radiation flux function and the radiation pressure function are defined at cell interfaces. One must properly upwind these two numerical functions to ensure stability and convergence toward the weak solution. This can be done here again using the Lax-Friedrich flux function, in which now the maximum wave speed can be chosen equal to the speed of light (Aubert & Teyssier 2008). We have, for example, for the flux function in the x-direction

$$F_x = \frac{(F_x)_L + (F_x)_R}{2} - \frac{c}{2}(E_R - E_L) \tag{76}$$

and for the first component of the pressure tensor

$$P_{xx} = \frac{(P_{xx})_L + (P_{xx})_R}{2} - \frac{c}{2}\left[(F_x)_R - (F_x)_L\right]. \tag{77}$$

We can analyze this numerical scheme the same way we did for the HD and MHD equations, namely that the leading error in this first-order Godunov scheme is exactly similar to a diffusion operator with numerical diffusion coefficient

$$\nu_{\rm num} = \frac{c\,\Delta x}{2}, \tag{78}$$

where here c is the speed of light. In a regime in which radiation is essentially transported at the speed of light, where the source terms are small compared with the advection terms, this numerical diffusion operator is small and vanishes as fast as the resolution of the grid. However, for problems in which source terms become stiff, this numerical diffusion term becomes problematic. We address this problem in Section 6, which is dedicated to numerical techniques for solving the HD, MHD, and RHD equations with source terms.

When coupling RT to HD with these methods, an additional problem arises because of the very large value of the speed of light compared with the fluid velocity. As we have said already, this is especially true for nonrelativistic flows. There are basically three possible strategies to solve this problem. If one decides to use an explicit time integration, in which the update of the radiation energy is performed using

$$\frac{E^{n+1} - E^n}{\Delta t} + \nabla \cdot F^n = 0, \tag{79}$$

where the flux function is given by the Lax-Friedrich formula with all variables evaluated at time n, then the maximum allowed time step for the RHD solver is governed by $\Delta t < \Delta x/c$, which can be very small, leading to an unrealistically large number of time steps. To alleviate this problem, one can either (*a*) reduce the speed of light artificially, leading to the so-called reduced speed of light approximation or slow light approximation (see, e.g., Gnedin & Abel 2001), which is a valid approach as long as the new (artificially increased) light crossing time is still smaller than all other timescales in the problem of interest (Rosdahl et al. 2013), or (*b*) accept the enlarged number of time steps and try to speed up the calculations using fast hardware solutions such as graphical processing units. A third strategy is to rely on implicit time integration, which is discussed in Section 6. This last technique is probably the most robust approach (see, for example, Jiang et al. 2012). However, it requires large sparse matrix manipulations and iterative schemes that can converge poorly in the case of highly nonstationary RHD flows.

The numerical methods we have reviewed so far in Section 4.3 are all grid based and are, therefore, ideally suited for coupling to grid-based HD codes. Many other popular techniques are available in the computational astrophysics literature. Although they may be considered as less natural and/or less efficient for coupling, they are nevertheless interesting and complementary to

the pure grid-based approach. Ray-tracing methods, for example, have been coupled successfully with grid-based HD codes, using the so-called long characteristics method (Abel et al. 1999, Cen 2002, Susa 2006) or the popular short characteristics method (Nakamoto et al. 2001, Mellema et al. 2006, Whalen & Norman 2006). Variants of the long characteristics method have been developed using adaptive ray tracing (Abel & Wandelt 2002, Razoumov & Cardall 2005, Wise & Abel 2011), whereas variants of the short characteristics techniques involve tessellation cones (Pawlik & Schaye 2008, 2011; Petkova & Springel 2011). A hybrid method, combining short and long characteristics, has been proposed by Rijkhorst et al. (2006) in the context of adaptive meshes. Another class of methods, usually referred to as Monte Carlo radiation transfer, samples the radiation phase space using randomly generated photon packets that are moving away from the source and being scattered randomly by the fluid elements (Altay et al. 2008, Baek et al. 2009, Cantalupo & Porciani 2011, Ciardi et al. 2001). Monte Carlo methods are usually harder to use with grid-based HD code, because of the inherent noise in the radiation field, but they are the only viable technique so far to deal accurately with subtle Doppler effects associated with line transfer.

5. ADDITIONAL HYDRODYNAMICAL PROCESSES

Solving only the Euler equations or the ideal MHD equations is not really useful for most astrophysical applications. One usually adds to these idealized equations several source terms, which is discussed in Section 6, but one can also add additional variables that could play an active role in the dynamics of the fluid. The first example of such additional processes comes when one wants to follow the detailed chemistry of the gas. This can be very simple, with only one chemical species like, for example, the metallicity of the cosmic gas, traditionally noted Z, which tracks the total mass fraction in all elements heavier than helium. This can be also very detailed and complicated, like typical chemistry networks used to model the physics of the ISM (see, e.g., Glover & Mac Low 2007). In any case, each chemical species is modeled using the mass fraction x^α for element α. Depending on the context, α can be various ionized species, such as HI, HII, or HeI, HeII, HeIII, together with the electrons. One can also follow various molecular species, such as CO, H_2O, H^2, or various nuclear reactions, at work in deep stellar interiors. For each species, one can write the evolution equation as

$$\frac{\partial \rho x^\alpha}{\partial t} + \nabla \cdot (\rho x^\alpha \mathbf{u}) = \mathcal{C}^\alpha - \mathcal{D}^\alpha. \tag{80}$$

We recognize here again the same structure with, on the left-hand side, the hyperbolic transport term and, on the right-hand side, the source terms, which are here classically expressed as $\mathcal{C}^\alpha$, the creation terms, and $\mathcal{D}^\alpha$, the destruction terms. The numerical approximation for the hydrodynamical flux is again based on the Riemann solver approach, and one can use again the Lax-Friedrich flux with

$$(F_x)^\alpha = \frac{\rho_L u_L x_L^\alpha + \rho_R u_R x_R^\alpha}{2} - \frac{S_{\max}}{2}(\rho_R x_R^\alpha - \rho_L x_L^\alpha). \tag{81}$$

The source terms, especially in the context of chemical reactions, can be very stiff, and they have to be treated properly, as explained in Section 6. Note that these extra chemical variables have no direct impact on the flow. They can have an indirect effect by regulating the cooling properties of the gas, but the hyperbolic step is not affected directly by the chemical species. These variables are called in this case passive scalars.

Another type of additional HD variables includes possible sources of nonthermal energy. Cosmic rays, for example, can be modeled as an additional energy variable, together with an additional pressure term in the Euler equation (Jubelgas et al. 2008, Enßlin et al. 2011). Radiation in the optically thick limit can also be modeled as an extra energy term and provides an extra pressure term

(Stone et al. 1992, Krumholz et al. 2007, Commercon et al. 2011b). Note that these additional energies are attached not to the gas particles but to other types of particles that are considered "trapped" in the fluid. The underlying assumption is that friction or absorption and re-emission among the gas particles and this other type of particles are so fast and efficient that they move with the fluid. In this case, one can model these nonthermal energies as

$$\frac{\partial e^{\beta}}{\partial t} + \nabla \cdot \left(e^{\beta}\mathbf{u}\right) = -P^{\beta}\nabla \cdot \mathbf{u} \quad \text{with} \quad P^{\beta} = (\gamma^{\beta} - 1)e^{\beta}, \tag{82}$$

where we have introduced the new variables e^{β}, P^{β}, and γ^{β} as the nonthermal energy, nonthermal pressure, and nonthermal adiabatic index, respectively. In the previous equation, we assume that this nonthermal energy is governed by an ideal EOS with a specified adiabatic exponent. Both cosmic rays and photons are relativistic particles with $\gamma^{\mathrm{CR}} = 4/3$ and $\gamma^{\mathrm{rad}} = 4/3$. It has also been proposed in recent models of subgrid, unresolved turbulence to model nonthermal energy using an additional energy equation and $\gamma^{\mathrm{turb}} = 5/3$ (Schmidt et al. 2006, Schmidt & Federrath 2011). All these extra nonthermal energies e^{CR}, e^{rad}, and e^{turb} can be added to the HD or MHD systems, increasing the realism of the simulation. The fundamental difference with the chemical variables is that these extra variables have potentially an influence on the dynamics of the flow through their corresponding pressure terms. Therefore, one has to modify the HD equations accordingly:

$$\frac{\partial \rho \mathbf{u}}{\partial t} + \nabla \cdot (\rho \mathbf{u} \otimes \mathbf{u} + P_{\mathrm{tot}}\mathbb{I}) = 0 \tag{83}$$

and

$$\frac{\partial E_{\mathrm{tot}}}{\partial t} + \nabla \cdot [\mathbf{u}(E_{\mathrm{tot}} + P_{\mathrm{tot}})] = 0; \tag{84}$$

and we have now for the total energy and total pressure

$$E_{\mathrm{tot}} = \rho\epsilon + \frac{1}{2}\rho \mathbf{u} \cdot \mathbf{u} + e^{\beta} \quad \text{and} \quad P_{\mathrm{tot}} = P + P^{\beta}. \tag{85}$$

Introducing these extra nonthermal energy variables has a direct impact on the Riemann solvers, because the flux functions have to be modified. The sound speed must also be modified as

$$c_s = \sqrt{\frac{\gamma P + \gamma^{\beta} P^{\beta}}{\rho}}. \tag{86}$$

We can now summarize the model equations that we have to solve to model astrophysical fluid flows, ignoring all the source terms, and focus only on the hyperbolic transport terms:

$$\frac{\partial \rho}{\partial t} + \nabla \cdot (\rho \mathbf{u}) = 0, \tag{87}$$

$$\frac{\partial \rho \mathbf{u}}{\partial t} + \nabla \cdot (\rho \mathbf{u} \otimes \mathbf{u} - \mathbf{B} \otimes \mathbf{B} + P_{\mathrm{tot}}\mathbb{I}) = 0, \tag{88}$$

$$\frac{\partial \mathbf{B}}{\partial t} - \nabla \times (\mathbf{u} \times \mathbf{B}) = 0, \tag{89}$$

$$\frac{\partial E_{\mathrm{tot}}}{\partial t} + \nabla \cdot [\mathbf{u}(E_{\mathrm{tot}} + P_{\mathrm{tot}}) - \mathbf{B}\,(\mathbf{B} \cdot \mathbf{u})] = 0, \tag{90}$$

$$\frac{\partial e^{\beta}}{\partial t} + \nabla \cdot \left(e^{\beta}\mathbf{u}\right) + P^{\beta}\nabla \cdot \mathbf{u} = 0, \tag{91}$$

$$\frac{\partial \rho x^{\alpha}}{\partial t} + \nabla \cdot (\rho x^{\alpha}\mathbf{u}) = 0, \tag{92}$$

with the additional definitions for the total fluid energy,

$$E_{\rm tot} = \rho\epsilon + \frac{1}{2}\rho\mathbf{u}\cdot\mathbf{u} + \frac{1}{2}\mathbf{B}\cdot\mathbf{B} + e^{\beta}, \tag{93}$$

and the total fluid pressure,

$$P_{\rm tot} = P + \frac{1}{2}\mathbf{B}\cdot\mathbf{B} + P^{\beta}, \tag{94}$$

and the equations of state,

$$P = (\gamma - 1)\rho\epsilon, \quad P^{\beta} = (\gamma^{\beta} - 1)e^{\beta}. \tag{95}$$

In parallel, one must solve for the transport of radiation using the two moment equations,

$$\frac{\partial E_{\nu}}{\partial t} + \nabla\cdot\mathbf{F}_{\nu} = 0 \tag{96}$$

and

$$\frac{\partial \mathbf{F}_{\nu}}{\partial t} + c^2\nabla\cdot\mathbb{P}_{\nu} = 0. \tag{97}$$

As we have already mentioned, very important terms are missing from these equations; they are not pure hyperbolic transport operators but play a fundamental role in the physics of astrophysical fluid flows. These are cooling and heating terms, radiation pressure terms, and microscopic diffusion processes (viscosity, thermal diffusion, magnetic resistivity, cosmic rays and trapped photon diffusion, chemical reactions. . .). All these processes are grouped into one single name, the source terms, because they do not participate directly in the numerical schemes we have described in the previous sections so far. We are now devoting an entire section to their numerical implementation.

6. SOURCE TERMS

In practical terms, source terms traditionally refer to everything that one can add to the right-hand side of the previous set of equations. We have already seen some examples, but we have not described the various numerical methods that are necessary to solve these terms properly. In a rather formal way, it is possible to describe the problem of source terms as a general equation of the form

$$\frac{\partial \mathbf{U}}{\partial t} + \nabla\cdot\mathbf{F}(\mathbf{U}) = \mathbf{S}(\mathbf{U}), \tag{98}$$

where $\mathbf{U}$ is the vector of conservative variables, $\mathbf{F}$ is the hyperbolic flux, and $\mathbf{S}$ is the vector of source terms. It is sometimes possible to approximate the source terms as a relaxation process toward an equilibrium state, i.e., as

$$\mathbf{S}(\mathbf{U}) = \frac{\mathbf{U}_{\rm eq} - \mathbf{U}}{\tau}, \tag{99}$$

where the equilibrium state is defined as the set of conservative variables satisfying

$$\mathbf{S}(\mathbf{U}_{\rm eq}) = 0. \tag{100}$$

The characteristic timescale τ is a measure of how fast the relaxation toward equilibrium is. A more accurate measurement of these timescales is given by the Jacobian matrix of the source function, defined as

$$\mathbb{J}(\mathbf{U}) = \frac{\partial \mathbf{S}}{\partial \mathbf{U}} \quad \text{and} \quad \frac{1}{\tau} = \mathrm{Tr}(\mathbb{J}). \tag{101}$$

We have to distinguish two regimes when we couple these source terms to the previously described hyperbolic solvers. These two regimes are divided according to the typical timescale associated

with the HD solver, namely

$$\Delta t_{\rm HD} = \frac{\Delta x}{S_{\rm max}}. \tag{102}$$

1. $\tau \gg \Delta t_{\rm HD}$: The physical processes associated with the source terms are very slow compared with the typical speed of HD or MHD waves in the flow. In this case, one can easily solve the source terms using the so-called operator splitting approach.
2. $\tau \leq \Delta t_{\rm HD}$: The source terms are now called stiff source terms, and one needs to be very careful about how to couple them to the HD routines.

6.1. Operator Splitting

In the nonstiff regime, source terms are a slow perturbation to the pure hyperbolic transport equations. In this case, the most simple method is to split the overall equations into two successive steps, the first step being the hyperbolic solver without source terms:

$$\frac{\tilde{\mathbf{U}}^{n+1} - \mathbf{U}^n}{\Delta t} + \nabla \cdot \mathbf{F}(\mathbf{U}^n) = 0, \tag{103}$$

where the temporary state $\tilde{\mathbf{U}}^{n+1}$ is updated in a second explicit step using

$$\frac{\mathbf{U}^{n+1} - \tilde{\mathbf{U}}^{n+1}}{\Delta t} = \mathbf{S}(\mathbf{U}^n). \tag{104}$$

Note that the source term update was performed using the initial state $\mathbf{U}^n$, which results in a scheme that is first-order accurate in time. This choice can be quite important, because if the solution is close to a stationary state, the previous simple method preserves it at the end of the two steps. Indeed, if one has

$$\nabla \cdot \mathbf{F}(\mathbf{U}^n) = \mathbf{S}(\mathbf{U}^{\rm n}), \tag{105}$$

then the previous scheme trivially results in

$$\frac{\mathbf{U}^{n+1} - \mathbf{U}^n}{\Delta t} = 0, \tag{106}$$

which is a very desirable property. One can also choose other implementations of the source term step, depending on the properties of the solution that we would like to recover. For stiff source terms (see Section 6.2), one can use the first-order implicit scheme, which reads as

$$\frac{\mathbf{U}^{n+1} - \tilde{\mathbf{U}}^{n+1}}{\Delta t} = \mathbf{S}(\mathbf{U}^{n+1}). \tag{107}$$

This requires us to solve for the unknown $\mathbf{U}^{n+1}$ using root-finding algorithms for possibly highly nonlinear equations. Note that this formulation does not preserve the stationary state unless one includes also the hyperbolic step in one single hyperbolic + source term implicit step:

$$\frac{\mathbf{U}^{n+1} - \mathbf{U}^n}{\Delta t} + \nabla \cdot \mathbf{F}(\mathbf{U}^{n+1}) = \mathbf{S}(\mathbf{U}^{n+1}). \tag{108}$$

This is obviously not an operator splitting approach anymore. A second-order accurate variant of the operator splitting approach would look like

$$\frac{\mathbf{U}^{n+1} - \tilde{\mathbf{U}}^{n+1}}{\Delta t} = \frac{\mathbf{S}(\mathbf{U}^{n+1}) + \mathbf{S}(\mathbf{U}^n)}{2}, \tag{109}$$

which may again require us to invert the right-hand side to find the final state. We now describe practical implementation of these general ideas for specific examples of source terms in astrophysical fluid flows.

6.2. Stiff Local Source Terms: Thermochemistry

When the Jacobian matrix of the source terms becomes very stiff, explicit schemes require very small time steps to be stable. However, it is desirable to maintain the HD time step to the relatively large value set by the Courant condition, namely

$$\Delta t_{\rm HD} \leq \frac{\Delta x}{S_{\rm max}}. \tag{110}$$

The classic strategy in this case is to rely on the operator splitting approach, using an implicit scheme for the second source terms–related update. This method works very well for complex chemical reaction networks and for cooling and heating processes. This is usually referred to as the thermochemistry step. In this case, the source terms are purely local; after the hydro step, cells can be treated independently. In each cell, one solves a set of ordinary differential equations featuring very small timescales that are much smaller that the global hydro time step $\Delta t_{\rm HD}$.

Many libraries have been developed to solve such stiff systems of ordinary differential equations. Recently published examples are KROME (Grassi et al. 2014) and GRACKLE (Bryan et al. 2014). They are usually based on an implicit scheme, which boils down to finding $\mathbf{U}^{n+1}$ as the root of this nonlinear equation,

$$\frac{\mathbf{U}^{n+1} - \mathbf{U}^{n}}{\Delta t} = \mathbf{S}(\mathbf{U}^{n+1}). \tag{111}$$

Root finding is traditionally performed for nonlinear functions using the Raphson-Newton method, an iterative technique that approximates the new solution at each step using a linear local approximation of the source function. This translates into the following iterative sequence,

$$\mathbf{U}^{p+1} = \mathbf{U}^{p} + \left[\mathbb{I} - \Delta t \mathbb{J}(\mathbf{U}^{p})\right]^{-1} \left[\Delta t \mathbf{S}(\mathbf{U}^{p}) - (\mathbf{U}^{p} - \mathbf{U}^{n})\right], \tag{112}$$

where we have $\mathbf{U}^{0} = \mathbf{U}^{n}$ and $\mathbf{U}^{\infty} = \mathbf{U}^{n+1}$. A common practice is to replace in the previous equation the Jacobian matrix with an approximation of the Jacobian matrix that is much faster to invert. For chemical reactions, it is customary to replace the Jacobian matrix by the sum of its diagonal matrix and its upper triangular matrix, $\mathbb{J} \simeq \mathbb{D} + \mathbb{U}$. Inversion is straightforward in this case because it requires a direct pivot elimination in each row (Press et al. 1992).

If the iterative sequence still converges, it converges toward the correct solution. The risk is that if the approximation is too crude, the scheme converges very slowly or even not at all. In this case, one uses a very powerful approach called subcycling. The idea is to break down the HD time step, $\Delta t_{\rm HD}$, into smaller substeps, Δt, set by the stiff solver. The size of the stiff time step is set by the requirement that the final increments of the variables stay small enough so that the Newton-Raphson iterations converge no matter what. This is called the 10% rule, which for each variable U_i is

$$\left|U_i^{n+1} - U_i^{n}\right| \leq 10\% U_i^{n}. \tag{113}$$

If the variation is smaller than that, one can increase the stiff time step; if it is larger, one should reduce the time step and go back to the previous step. For most applications, using the 10% rule allows one to reduce the number of Raphson-Newton iterations to a few or even only one. The overall implicit scheme is very fast and robust.

6.3. Relaxation Toward the Equilibrium State

We have described a powerful numerical technique to deal with stiff source terms in each cell independently. However, we have not analyzed the consequence of such a scheme to the coupled HD + source terms set of equations. A classic example in astrophysics is when one has cooling

and heating terms, due to radiative processes, in the energy equations. For the sake of simplicity, we write the energy equation as

$$\frac{\partial E}{\partial t} + \nabla \cdot [\mathbf{u}(E + P)] = \Gamma_{\rm rad} - \Lambda_{\rm rad} \simeq \rho \frac{\epsilon_{\rm eq} - \epsilon}{\tau}, \tag{114}$$

where ϵ is the gas specific energy, $\epsilon_{\rm eq}$ is the equilibrium value set by the microscopic processes, and τ is the relaxation timescale. When thermal equilibrium is reached, the gas internal energy is set to its equilibrium value. The previous energy equation becomes irrelevant, and the previous hyperbolic system relaxes toward the isothermal Euler equations, which feature only mass and momentum conservation,

$$\frac{\partial \rho}{\partial t} + \nabla \cdot (\rho \mathbf{u}) = 0 \tag{115}$$

and

$$\frac{\partial \rho \mathbf{u}}{\partial t} + \nabla \cdot \left(\rho \mathbf{u} \otimes \mathbf{u} + P_{\rm eq} \mathbb{I}\right) = 0, \tag{116}$$

where the equilibrium pressure depends only on density,

$$P_{\rm eq} = (\gamma - 1)\rho \epsilon_{\rm eq} = \rho c_{\rm iso}^2. \tag{117}$$

For the isothermal Euler equation, the sound speed is indeed given by $c_{\rm iso} = \sqrt{P/\rho}$, whereas for the adiabatic case, the sound speed is larger with $c_s = \sqrt{\gamma P/\rho}$. If now one uses the operator splitting approach and the Lax-Friedrich numerical flux based on the adiabatic sound speed, this results in a numerical diffusion term for both the mass and momentum conservation equations; by contrast, if τ is much smaller than $\Delta t_{\rm HD}$, one should use the Lax-Friedrich scheme based on the isothermal sound speed, as it should be in the relaxed system, namely the isothermal Euler equations.

The price to pay when one couples the adiabatic Euler equations to a stiff source term in the operator splitting approach is, therefore, excessive numerical diffusion (by a factor of $\sqrt{\gamma}$). Although this is not really a problem for most applications, there is an elegant way to solve the issue that was first proposed by Liu (1987), which is very useful in designing numerical schemes for stiff source terms under many circumstances that can be much more dramatic (see Sections–6.4–6.6). The methodology, similar to the Chapman-Enskog procedure in the theory of gases, relies on noting that the energy equation first relaxes to the stationary solution to first order in the small parameter τ. Neglecting the time derivative in the energy equation, we find that the gas pressure is

$$P \simeq P_{\rm eq} - (\gamma - 1)\tau \nabla \cdot \left[\mathbf{u}\left(E_{\rm eq} + P_{\rm eq}\right)\right]. \tag{118}$$

The second term on the right-hand side is equivalent to a viscous pressure for which the (small) viscous timescale is equal to the cooling time. From now on, for the sake of simplicity, we restrict ourselves to one-dimensional subsonic flows. The first-order asymptotic regime we just derived can be approximated as

$$\frac{\partial \rho u}{\partial t} + \frac{\partial}{\partial x}\left(P_{\rm eq}\right) = \frac{\partial}{\partial x}\left(\gamma \tau c_{\rm iso}^2 \frac{\partial \rho u}{\partial x}\right). \tag{119}$$

We now want to construct a numerical flux function that works in both regimes: in the adiabatic regime, in which $\tau \gg \Delta x\, c_{\rm iso}$ and

$$F_{\rm adiab} \simeq \frac{P_L + P_R}{2} - \frac{c_{\rm adiab}\Delta x}{2}\left(\frac{\rho_R u_R - \rho_L u_L}{\Delta x}\right), \tag{120}$$

and in the isothermal regime, in which $\tau \ll \Delta x\, c_{\rm iso}$ and

$$F_{\rm iso} \simeq \frac{P_L + P_R}{2} - \frac{c_{\rm iso}\Delta x}{2}\left(\frac{\rho_R u_R - \rho_L u_L}{\Delta x}\right). \tag{121}$$

We try to interpolate between regimes, with an unknown function of the flow variables $0 < f < +\infty$, such that

$$F_{\rm stiff} = \frac{1}{1+f}F_{\rm iso} + \frac{f}{1+f}F_{\rm adiab}. \tag{122}$$

In our asymptotic quasi-isothermal regime, we have

$$F_{\rm stiff} \simeq F_{\rm iso} + f\,(F_{\rm adiab} - F_{\rm iso}). \tag{123}$$

Identifying the second term on the right-hand side with the viscous pressure of the exact asymptotic regime, we find

$$f = \frac{2\gamma}{\sqrt{\gamma}-1}\frac{c_{\rm iso}\tau}{\Delta x}. \tag{124}$$

Our final numerical scheme uses a simple interpolation between the adiabatic and the isothermal Riemann solvers. The interpolation function we derived allows us to recover the exact asymptotic solution of the underlying set of equations. We therefore relax toward the isothermal Euler equations with the correct asymptotic solution. Note that this methodology can be generalized to the supersonic case too.

As we have said already, this very careful treatment of the HD in the presence of stiff source terms allows one to design a numerical technique with minimal numerical diffusion. In practice, this is probably too much given the overall accuracy of first-order or even second-order methods. However, we have introduced a very important number that measures the stiffness of the relaxation processes with respect to the maximum wave speed $S_{\rm max}$ of the hyperbolic transport, namely the Peclet number:

$$\mathrm{Pe} = \frac{\Delta x}{S_{\rm max}\tau}. \tag{125}$$

If $\mathrm{Pe} < 1$, then the source terms are slow enough, and one can ignore what we have just discussed. The operator splitting approach is sufficiently accurate using classic adiabatic Riemann solvers. If $\mathrm{Pe} > 1$, the source terms become stiff, and adiabatic Riemann solvers must be modified to account for the source terms and avoid excessive numerical diffusion.

6.4. Radiation Transport Source Terms

We now describe another example of stiff source terms in which the consequences of operator splitting are much more dramatic than the case discussed in Section 6.3. The source terms in the frequency integrated radiation moment equations are

$$\frac{\partial E}{\partial t} + \nabla\cdot \mathrm{F} = \frac{aT^4 - E}{\tau} \tag{126}$$

and

$$\frac{\partial \mathrm{F}}{\partial t} + c^2\nabla\cdot\mathbb{P} = \frac{-\mathbf{F}}{\tau}/, \tag{127}$$

where a is the Stefan-Boltzmann constant, $\tau = \lambda/c$ is the matter-radiation coupling timescale, and λ is the frequency-averaged mean free path.

In the optically thick limit, for which one has $\lambda \ll \Delta x$, the radiation source terms become stiff compared with the transport timescale $\Delta t_{\mathrm{RT}} = \Delta x/c$. We can use here again the Chapman-Enskog methodology and analyze the stationary state to first order in the small parameter λ. The second moment equation gives a stationary state for which the radiation flux is quite small, of order $c\lambda$, whereas the first equation results in a radiation energy than can be large, of order aT^4. We can conclude immediately that, in this regime, the Eddington tensor is isotropic and $\mathbb{P} = (E/3)\mathbb{I}$. The second moment equation thus gives us an asymptotic regime called the diffusion limit (Mihalas & Mihalas 1984), where

$$\mathbf{F} = -\frac{c\lambda}{3}\nabla E, \tag{128}$$

and we are left with only the energy equation, which is a classic diffusion operator,

$$\frac{\partial E}{\partial t} - \frac{c\lambda}{3}\Delta E = \frac{aT^4 - E}{\tau}. \tag{129}$$

Let us now examine how our numerical scheme relaxes to this asymptotic diffusion regime. We now understand, from our previous analysis, that the first Godunov scheme with the Lax-Friedrich numerical flux results in an ME of the form

$$\frac{\partial E}{\partial t} + \nabla \cdot \mathbf{F} - \nu_{\mathrm{num}}\Delta E = \frac{aT^4 - E}{\tau} \tag{130}$$

and

$$\frac{\partial \mathbf{F}}{\partial t} + c^2\nabla \cdot \mathbb{P} - \nu_{\mathrm{num}}\Delta \mathbf{F} = \frac{-\mathbf{F}}{\tau}, \tag{131}$$

where the numerical diffusion is $\nu_{\mathrm{num}} = c\Delta x/2$. Here again, for a small mean free path, the radiation flux asymptotically vanishes compared with the radiation energy. But the ME for the radiation energy is now

$$\frac{\partial E}{\partial t} - \frac{c\lambda}{3}\Delta E - \frac{c\Delta x}{2}\Delta E = \frac{aT^4 - E}{\tau}. \tag{132}$$

We see that in the diffusion limit, for which $\Delta x \gg \lambda$, the numerical diffusion completely overwhelms the physical diffusion term. The resulting numerical scheme is, therefore, inaccurate to zeroth order, as diffusion proceeds with an effective mean free path equal to the cell size.

Using high-order transport schemes for the radiation improves the situation, as the numerical diffusion term would be much smaller in this case, but they eventually break for a small enough mean free path. This is one dramatic consequence of using the operator splitting approach on stiff source terms. We see that the numerical diffusion becomes larger than the physical diffusion if

$$\frac{c\lambda}{3} < \frac{c\Delta x}{2} \quad \text{or} \quad \mathrm{Pe} = \frac{\Delta x}{c\tau} > \frac{2}{3}. \tag{133}$$

Here again, the Peclet number is a measure of the stiffness of the source terms, compared with the hyperbolic solver.

An elegant solution to this problem was proposed by Berthon et al. (2006), who followed the methodology of Bouchut (2004). These authors designed a Riemann solver that explicitly takes into account the source terms. The mathematical derivation is quite involved, but the final result can be approximated as a simple modification of the Lax-Friedrich flux function,

$$F_{\mathrm{num}} = \frac{F_L + F_R}{2} - \frac{c}{2}\left(E_R - E_L\right), \tag{134}$$

where the left and right states are all multiplied by a function α, defined as

$$\alpha_L = \frac{1}{1 + 3/2\,\mathrm{Pe}_L}. \tag{135}$$

For a small Peclet number, we get $\alpha \simeq 1$, and for a large Peclet number, the Lax-Friedrich numerical flux for the radiation energy becomes

$$F_{\mathrm{num}} \simeq \frac{2\lambda}{3\Delta x}\frac{F_L + F_R}{2} - \frac{c\lambda}{3}\frac{E_R - E_L}{\Delta x}, \tag{136}$$

which now has the correct asymptotic limit. Note that this solution, although justified by a nonlinear analysis of the generalized Riemann problem, is in practice very similar to the relaxation scheme we used for the isothermal Euler equations.

6.5. Gravity Source Terms

Gravity is probably the most important source term for astrophysical applications. It is the prototypical external force field one uses in fluid mechanics courses dealing with the Euler equations. One can also regroup in the same category centrifugal forces, Coriolis forces, and various additional geometrical terms that are caused by frame transformations. The gravity force is given by the gradient of the gravitational potential, which is related to the gas density through the Poisson equation

$$\mathbf{F}_{\mathrm{grav}} = -\rho\nabla\phi \quad \text{with} \quad \Delta\phi = 4\pi G\rho. \tag{137}$$

Gravity is added as a source term in the HD equations,

$$\frac{\partial\rho\mathbf{u}}{\partial t} + \nabla\cdot(\rho\mathbf{u}\otimes\mathbf{u} + P\mathbb{I}) = \mathbf{F}_{\mathrm{grav}}, \tag{138}$$

$$\frac{\partial E}{\partial t} + \nabla\cdot[\mathbf{u}(E+P)] = \mathbf{F}_{\mathrm{grav}}\cdot\mathbf{u}. \tag{139}$$

The right-hand side of the energy equation is the work of the gravitational force. These two source terms can be implemented numerically using here again the operator split approach, in which updating the source terms would be performed just after the hyperbolic update as either a first-order scheme,

$$\frac{(\rho\mathbf{u})^{n+1} - (\rho\mathbf{u})^n}{\Delta t} = -\rho^n(\nabla\phi)^n, \tag{140}$$

$$\frac{(E)^{n+1} - (E)^n}{\Delta t} = -\rho^n(\nabla\phi)^n\cdot\mathbf{u}^n, \tag{141}$$

or a second-order version,

$$\frac{(\rho\mathbf{u})^{n+1} - (\rho\mathbf{u})^n}{\Delta t} = -\frac{\rho^n(\nabla\phi)^n + \rho^{n+1}(\nabla\phi)^{n+1}}{2}, \tag{142}$$

$$\frac{(E)^{n+1} - (E)^n}{\Delta t} = -\frac{\rho^n(\nabla\phi)^n\cdot\mathbf{u}^n + \rho^{n+1}(\nabla\phi)^{n+1}\cdot\mathbf{u}^{n+1}}{2}, \tag{143}$$

For the second-order scheme, the final update can only be performed after the new Poisson equation has been solved:

$$\Delta\phi^{n+1} = 4\pi G\rho^{n+1}. \tag{144}$$

As we have mentioned already above, for certain applications it is critical to enforce strictly the stationary state. In the presence of gravity, the stationary state is often referred to as the hydrostatic equilibrium. It is defined as a static fluid with $\mathbf{u} = 0$ and

$$\frac{1}{\rho}\nabla P = -\nabla\phi. \tag{145}$$

Great care must be taken to enforce strictly this equilibrium in the numerical solution. Indeed, if one follows the classic Godunov methodology, assuming that the solution is piecewise constant, this results in very strong pressure gradients at cell interfaces, with no guarantee that they shall be cancelled exactly by the gravity source step. Several solutions have been proposed in the astrophysics literature. A very simple technique proposed recently by Käppeli & Mishra (2014) consists of using different fluid variables, namely the gas specific enthalpy $h = \epsilon + p/\rho$ and the gas specific entropy s. A strict isentropic hydrostatic equilibrium can be enforced using $\nabla(h + \phi) = 0$ and $\nabla s = 0$. These new variables are, therefore, the new piecewise constant states that are used as input states in the Riemann solver. The gravity source terms are also modified so that they cancel the pressure gradient exactly.

A very controversial topic for self-gravitating flows is related to the numerical fragmentation of the gas, leading to the artificial suppression or, on the contrary, to the artificial formation of dense gas clumps in compressible self-gravitating turbulent flows. In a seminal paper, a simple numerical experiment on the formation of a dense isothermal filament was performed by Truelove et al. (1997), in which it was argued that one must resolve the Jeans length of the simulated gas by at least four cells to prevent artificial fragmentation of the filament. From our previous analysis, we know that the leading-order error in our various Godunov schemes was a diffusion operator, with a numerical diffusion coefficient $\nu_{\text{num}} = S_{\max}\Delta x/2$. It is possible to repeat here the classic Jeans analysis by linearizing the ME instead of the original isothermal Euler equations. We consider small perturbations, $\delta\rho$ and $\delta\mathbf{u}$, around a reference equilibrium state, $\rho_0, \mathbf{u}_0 = 0$, that satisfy the following linearized equations:

$$\frac{\partial(\delta\rho)}{\partial t} + \rho_0\nabla\cdot(\delta\mathbf{u}) = \nu_{\text{num}}\Delta(\delta\rho), \tag{146}$$

$$\frac{\partial(\delta\mathbf{u})}{\partial t} + \frac{c_{\text{iso}}^2}{\rho_0}\nabla(\delta\rho) = \nu_{\text{num}}\Delta(\delta\mathbf{u}) - \nabla\phi. \tag{147}$$

Taking the divergence of the second equation and noting $\delta\theta = \nabla\cdot(\delta\mathbf{u})$, one has

$$\frac{\partial(\delta\theta)}{\partial t} + \frac{c_{\text{iso}}^2}{\rho_0}\Delta(\delta\rho) = \nu_{\text{num}}\Delta(\delta\theta) - \Delta\phi = \nu_{\text{num}}\Delta(\delta\theta) - 4\pi G\delta\rho. \tag{148}$$

We are looking for plane wave solutions proportional to $\exp i(kx - \omega t)$. For wave numbers $k < k_{\text{J}}$, where

$$k_{\text{J}} = \frac{\sqrt{4\pi G\rho_0}}{c_{\text{iso}}}, \tag{149}$$

we obtained classic, damped sound waves. It is more convenient to refer here to the Jeans length, $\lambda_{\text{J}} = 1/k_{\text{J}}$. For larger scales, we obtain unstable modes only for scales larger than an effective Jeans length,

$$\tilde{k}_{\text{J}}^2 = k_{\text{J}}^2\frac{\sqrt{1 + \left(\frac{\Delta x}{\lambda_{\text{J}}}\right)^2} - 1}{\frac{1}{2}\left(\frac{\Delta x}{\lambda_{\text{J}}}\right)^2}. \tag{150}$$

This effective Jeans length is larger than the true Jeans length, which means that numerical diffusion spuriously stabilizes the flow. The previous relation states that the numerical Jeans length is increased by 10% if $\Delta x \simeq \lambda_J$, which is a very moderate effect. Artificial fragmentation has another origin, which has nothing to do with a linear instability analysis using a static, uniform, equilibrium reference state. What is likely to occur in a Jeans unstable flow is that singularities, in the density and velocity fields, are forming; numerical errors in those singularities are large and they grow later as a result of the Jeans instability. Therefore, artificial fragmentation proceeds more likely because of possible intrinsic unstable numerical behaviors as a result of those singularities rather than a spurious modification of the Jeans instability mechanism. Thus, resolving the Jeans length is required to attenuate these singularities and minimize numerical errors associated with them.

6.6. High–Mach Number Flows

A typical problem in astrophysical fluid simulations, most often in the presence of gravity, is the formation of highly supersonic flows with very strong velocity gradients. Under such extreme conditions, the computed gas internal energy can be completely wrong. Note than in such extremely supersonic cases, the gas pressure plays virtually no dynamical role, so that numerical errors in the pressure are also likely to play no role in the solution. However, if one needs the computed gas temperature to estimate the cooling rate or to perform chemical reactions, this can have a dramatic effect. In such cases, it is of great interest to find a solution for which the computed gas internal energy is properly estimated. In Godunov schemes, the gas internal energy is always computed by subtracting from the total energy the kinetic and magnetic energies,

$$e = E_{\rm tot} - \frac{1}{2}\rho u^2 - \frac{1}{2}B^2. \tag{151}$$

If both the kinetic energy and the magnetic energy dominate over the internal energy, one subtracts two very large, almost equal numbers, and the result of this subtraction is potentially affected by numerical errors. Note that this relation is precisely what leads to shock heating and reconnection heating in a conservative scheme, so this is a desirable property of our numerical scheme. This should happen mostly in shock fronts or in reconnection layers, leading to a fast heating of the gas, after which the gas internal energy becomes quickly high enough. In contrast, if the flow features large cold regions with strong velocity and magnetic fields gradients, without shocks or reconnection layers, the numerical scheme is likely to fail.

A simple way to estimate the magnitude of this effect is to compute the ME for the internal energy, restricting ourselves to one-dimensional flows. We have seen already that each of the four conservative variables $\mathbf{U} = (\rho, \rho\mathbf{u}, E, \text{and } \mathbf{B})$ satisfies a modified conservation law,

$$\frac{\partial \mathbf{U}}{\partial t} + \nabla \cdot \mathbf{F} = \nu_{\rm num} \Delta \mathbf{U}. \tag{152}$$

After some relatively simple algebra, one finds that the ME for the gas internal energy is

$$\frac{\partial e}{\partial t} + \nabla \cdot (e\mathbf{u}) + P\nabla \cdot \mathbf{u} = \nu_{\rm num} \left[\rho \left(\frac{\partial u}{\partial x} \right)^2 + \left(\frac{\partial B}{\partial x} \right)^2 \right]. \tag{153}$$

The good news is that here the important physical property that the entropy must always increase is reproduced, because the right-hand side of the previous equation, the leading-order error term for the internal energy, is always positive. The bad news is, however, that if the internal energy is very small, this term then dominates over the left-hand side, and the computed internal energy is likely unphysically large. For higher-order schemes, the situation is not as simple: The leading-order error term in the ME for the internal energy has a smaller magnitude and scales as Δx

to some power equal to the order of the scheme. But its sign is not strictly positive anymore. This could lead to negative temperatures if one uses the conservative update of the total fluid energy.

There is a solution to fix the internal energy variable in the case of highly supersonic velocity gradients; it is called the dual energy formulation of the Godunov scheme (Ryu et al. 1993, Bryan et al. 1995). The idea is to solve two equations in parallel for the internal energy, a conservative equation, that can lead to large truncation errors,

$$\frac{\partial E_{\rm tot}}{\partial t} + \nabla \cdot [\mathbf{u}(E_{\rm tot} + P_{\rm tot}) - \mathbf{B}\,(\mathbf{B} \cdot \mathbf{u})] = 0, \tag{154}$$

followed by

$$e = E_{\rm tot} - \frac{1}{2}\rho u^2 - \frac{1}{2}B^2 \tag{155}$$

and a nonconservative equation, for which there is no shock heating or reconnection heating but also no large induced errors:

$$\frac{\partial e}{\partial t} + \nabla \cdot (e\mathbf{u}) + P\nabla \cdot \mathbf{u} = 0. \tag{156}$$

A minimal internal energy for the conservative scheme can be evaluated, on the basis of our estimate of the local numerical truncation error,

$$e_{\rm trunc} = \nu_{\rm num}\Delta t \left[\rho \left(\frac{\partial u}{\partial x}\right)^2 + \left(\frac{\partial B}{\partial x}\right)^2\right]. \tag{157}$$

We now replace the partial derivatives of the velocity (and the magnetic field) by $\Delta u/\Delta x$, in which the Δu is the undivided difference of two neighboring velocities (and magnetic fields). Assuming that the Courant factor is close to unity, we end up with a simple estimate of the truncation error in each cell,

$$e_{\rm trunc} \simeq \frac{1}{2}\left[\rho\,(\Delta u)^2 + (\Delta B)^2\right]. \tag{158}$$

The dual energy formulation of the Godunov scheme can finally be summarized as follows:

1. We start at the beginning of the time step with the total fluid energy E^n and the fluid internal energy e^n.
2. We solve for the total energy update using the conservation law,

$$\frac{E^{n+1}_{\rm cons} - E^n}{\Delta t} = -\nabla \cdot \mathbf{F}(E)^n. \tag{159}$$

3. We compute from this total energy the new conservative internal energy using

$$e^{n+1}_{\rm cons} = E^{n+1}_{\rm cons} - \frac{1}{2}\rho^{n+1}(u^{n+1})^2 - \frac{1}{2}(B^{n+1})^2. \tag{160}$$

4. We also compute in parallel another internal energy variable using the nonconservative or primitive equation,

$$\frac{e^{n+1}_{\rm prim} - e^n}{\Delta t} = -\nabla \cdot \mathbf{F}(e)^n - P^n\nabla \cdot \mathbf{u}^n. \tag{161}$$

5. Finally, we test for whether the conservative internal energy update is larger than a fraction of our estimated truncation error in order to adopt it for the final update; otherwise, we use the nonconservative update,

$$\text{if} \quad e^{n+1}_{\rm cons} > \beta_{\rm dual} e_{\rm trunc}, \quad \text{then} \quad e^{n+1} = e^{n+1}_{\rm cons}, \tag{162}$$

$$\text{else} \quad e^{n+1} = e^{n+1}_{\rm prim}. \tag{163}$$

The free parameter, β_{dual}, can be set between 0 and 1, ideally equal to 1/2. If set too high, it could affect shock and reconnection heating in sharp shock front or reconnection sheets, leading to a degradation of the total energy conservation. If set too low, it won't remove spuriously heated regions, therefore defeating the purpose of the entire methodology. In strong shock waves and reconnection layers, it is important to realize that, after the conservative update, the conservative internal energy will in general be higher than our estimate of the truncation error, so that this dual energy update will not affect these important flow features. This dual energy formulation is particularly important in self-gravitating flow, in which gravity induces a supersonic velocity gradient. In cold discs, for example, the global Keplerian rotation also features strong gradients that result in a spurious heating of the gas. As we have stated several times already, the truncation error in the internal energy can be significantly reduced by increasing the resolution. The velocity undivided difference in smooth regions of the flow will decrease, as the mesh size is decreased, with ultimately no need for the dual energy approach, as soon as the resolution is high enough for the velocity gradients to become subsonic. However, it is not always possible to maintain a high-enough resolution. The truncation errors in the internal energy can also be used to adaptively refine the mesh, as we discuss now in Section 7.

7. MESH GEOMETRY

We have analyzed in great detail the properties of grid-based numerical algorithms for astrophysical fluid flows. We have shown that the HD or MHD equations can be solved numerically using the Godunov methodology, a very general framework now almost exclusively adopted by most astrophysical software. In this framework, it is easy to show that we are not solving the original equations exactly, of course, but we are in fact solving a modified set of equations that formally include an additional diffusion term dubbed the numerical diffusion. In the case of a first-order Godunov scheme with the Lax-Friedrich flux function, we found the corresponding numerical diffusion parameter to be

$$\nu_{\text{num}} \simeq \frac{S_{\max}\Delta x}{2}, \tag{164}$$

where $S_{\max}$ is the maximum wave speed estimated locally on the cell, and the corresponding diffusion operator is a classic Laplacian operator.

The goal of our numerical experiments is obviously to minimize the truncation errors in the computed solution, converging toward the weak solution of the underlying set of equations, while preserving the stability of the scheme. To achieve this, we need to minimize numerical diffusion, without suppressing it entirely, otherwise we risk finding a spurious, unphysical solution or generating undesired flow instabilities. We have already discussed higher-order schemes as a powerful way to minimize numerical errors. Higher-order schemes turn out to be very useful for smooth flows and devoid of discontinuities. In general, however, astrophysical flows are strongly compressible flows, and they feature many discontinuities, such as shocks, shearing, or reconnection layers, etc. Moreover, we have also seen that in the presence of stiff source terms, it is desirable to resolve the associated length scale to avoid spurious effects, so that going to higher order may help, but only up to a certain point.

From the previous equation, we see that we have basically two possible strategies to minimize numerical diffusion for low-order (first and second, say) numerical schemes: reducing the mesh size or reducing the maximum wave speed. The first possibility can be implemented using the so-called adaptive mesh refinement (AMR) technique. The second strategy can be obtained using a so-called moving mesh (MvM) or arbitrary Lagrangian Eulerian (ALE) technique. Both approaches have

been implemented in the astrophysical literature and have proven quite successful in providing high-quality numerical solutions.

7.1. Adaptive Mesh Refinement

The AMR technique was introduced by Berger & Oliger (1984) and Berger & Colella (1989) in a pure fluid dynamics solver using adaptively refined grids. It was introduced in astrophysics by Klein et al. (1994) to study shock-cloud interactions, taking advantage of the highly refined grid at the interface between the cloud and the interstellar medium. It was then adapted for self-gravitating cosmological flows roughly at the same time, by Bryan & Norman (1995), as the first introduction of the ENZO code. Many other codes have since been developed in the following years with applications ranging from thermonuclear flashes (Fryxell et al. 2000) to MHD simulations (Ziegler 1998, Nool & Keppens 2002) to galaxy formation (Kravtsov et al. 1997, Knebe et al. 2001, Teyssier 2002). We discuss all these packages in Section 8.

The basic idea of AMR is to refine the mesh adaptively in regions of the flow in which truncation errors (or equivalently numerical diffusion) are too large. There are two fundamental requirements for AMR algorithms: (*a*) the HD solver needs to be adapted to a complex mesh geometry, in which cells of different sizes (usually a factor of 2) have to coexist and exchange fluxes conservatively; (*b*) very careful refinement strategies must be developed to improve the quality of the solution and not degrade it. A natural idea for the latter is to use our estimate of the numerical truncation errors as a trigger for mesh refinements. In more mathematical terms, we want the truncation errors to be much smaller than the divergence of the flux, which can be interpreted most of the time as a convection term at the corresponding wave speed, namely $\nu_{\rm num}\Delta U \ll \nabla(SU)$. Using our formula for the numerical diffusion, this translates into the following refinement criterion:

$$\text{If} \quad \Delta x \left| \frac{\partial^2 U}{\partial x^2} \right| > C_1 \left| \frac{\partial U}{\partial x} \right|, \quad \text{then refine,} \tag{165}$$

where C_1 is a dimensionless constant that needs to be adjusted, depending on the required accuracy and the available resources. In presence of source terms, we have also derived a condition, based on the Peclet number $\mathrm{Pe} = \frac{\Delta x}{S\tau} < 1$, under which the operator splitting approach can work properly in which τ is the timescale associated with the source terms. This can also be translated into a refinement criterion:

$$\text{If} \quad \Delta x > C_2(|u| + c_s)\tau, \quad \text{then refine.} \tag{166}$$

RT codes can take advantage of refining the photon mean free path with several computational cells, for example. In the presence of stiff cooling, one can refine the grid so it samples the cooling length. A very popular refinement criterion is self-gravitating flows, which have to be derived from the previous idea, namely,

$$\text{If} \quad \Delta x > C_3\lambda_J, \quad \text{then refine,} \tag{167}$$

where $\lambda_{\rm J} = c_s t_{\rm ff}$ is the Jeans length. Another widely adopted refinement criterion for self-gravitating flows is to enforce a minimal mass per cell:

$$\text{If} \quad \Delta x > \left(\frac{m_{\rm min}}{\rho} \right)^{1/3}, \quad \text{then refine.} \tag{168}$$

This ensures that the source for gravity, namely the gravitational mass, is homogeneously distributed in the computational domain. This technique is also used to enforce a quasi-Lagrangian evolution of the mesh, because refined cells are following the mass in which it flows.

Our second requirement is to be able to implement the Godunov scheme with adaptively refined cells. This is the heart of the AMR technique for HD solvers. The main steps to follow are described here:

1. At the interface between coarse and fine cells, the coarse numerical fluxes have to be replaced by the sum of all fine numerical fluxes. This step is called flux correction. For the induction equation in MHD solvers, we also need to perform a coarse-fine electric field correction at cell edges.
2. At the interface between coarse and fine cells, we need to compute appropriate boundary conditions for the fine domain, interpolating coarse values from the coarse domain. This interpolation step is crucial, as it is also used when one needs to create new cells when new refinements are required.
3. Although refined (or split) cells are not directly useful for the flow solver, as we want to discard the solution there, we still need to average flow variables over fine cells when we want to derefine the grid. This last step is usually taken as the transpose of the interpolation operator.

A fundamental issue to address when designing proper refinement strategy is to choose the variables over which one performs various averaging and interpolating steps. Although one may naïvely expect that the conservative variables (mass, momentum, and total energy) should always be used, it is not the case for supersonic, self-gravitating flows. Averaging and interpolating the total fluid energy affects strongly the gas internal energy. Strong velocity gradients shall cause a spurious turbulent heating, because we lose the information of the unresolved supersonic turbulence. One solution is to refine the grid everywhere the velocity gradients are supersonic, therefore alleviating our previously discussed problems with internal energy truncation errors without using the dual energy formulation and minimizing the effect of turbulent heating when derefining the grid. Another solution is to keep track of the unresolved turbulent energy in a new, nonthermal energy variable, as explained in Section 5 (see, e.g., Schmidt & Federrath 2011). The cheapest solution is to use the gas internal energy as the interpolation variable, giving up on strict conservation but obtaining a more correct solution for the gas temperature.

7.2. Moving Mesh

The second class of mesh adaptation techniques that can be used to minimize numerical diffusion is based on moving the cells in a quasi-Lagrangian way. We can distinguish the Eulerian version of the HD equations,

$$\frac{\partial \rho}{\partial t} + \nabla \cdot (\rho \mathbf{u}) = 0, \tag{169}$$

$$\frac{\partial \rho \mathbf{u}}{\partial t} + \nabla \cdot (\rho \mathbf{u} \otimes \mathbf{u} + P\mathbb{I}) = 0, \tag{170}$$

and

$$\frac{\partial E}{\partial t} + \nabla \cdot (E + P)\mathbf{u} = 0, \tag{171}$$

to the Lagrangian formulation,

$$\frac{1}{\rho}\frac{D\rho}{Dt} + \nabla \cdot \mathbf{u} = 0, \tag{172}$$

$$\rho \frac{D\mathbf{u}}{Dt} + \nabla \cdot P\mathbb{I} = 0, \tag{173}$$

and

$$\rho \frac{D}{Dt}\left(\frac{E}{\rho}\right) + \nabla \cdot P\mathbf{u} = 0, \tag{174}$$

where $D\alpha/Dt$ stands for the Lagrange derivative of a scalar quantity α,

$$\frac{D\alpha}{Dt} = \frac{\partial \alpha}{\partial t} + \mathbf{u} \cdot \nabla \alpha. \tag{175}$$

There is also an intermediate version of the HD equations, usually referred to as the ALE approach, in which we define a grid velocity, $\mathbf{w}$, that is not necessarily equal to the grid velocity. We can write the Euler equations in conservative form, using as the volume element the grid cell V (see, e.g., Springel 2010a):

$$\frac{\mathrm{d}}{\mathrm{d}t}\int_V \rho \mathrm{d}V = -\int_S \rho(\mathbf{u}-\mathbf{w})\cdot \mathbf{n}\mathrm{d}S, \tag{176}$$

$$\frac{\mathrm{d}}{\mathrm{d}t}\int_V \rho\mathbf{u}\mathrm{d}V = -\int_S \rho\mathbf{u}(\mathbf{u}-\mathbf{w})\cdot \mathbf{n}\mathrm{d}S - \int_S P\mathbf{n}\mathrm{d}S, \tag{177}$$

$$\frac{\mathrm{d}}{\mathrm{d}t}\int_V E\mathrm{d}V = -\int_S E(\mathbf{u}-\mathbf{w})\cdot \mathbf{n}\mathrm{d}S - \int_S P\mathbf{u}\cdot \mathbf{n}\mathrm{d}S, \tag{178}$$

where now the cell's volume element evolves according to the grid velocity,

$$\frac{\mathrm{d}V}{\mathrm{d}t} = \int_V (\nabla \cdot \mathbf{w})\mathrm{d}V\,. \tag{179}$$

Note that in this general ALE formulation, mass, momentum, and total energy inside the cells are also strictly conserved. The only source of numerical diffusion comes from the pressure terms, which is associated with the sound waves, and from the relative velocity between the fluid and the grid. The associated numerical diffusion coefficient is (assuming here again the Lax-Friedrich flux function)

$$\nu_{\mathrm{num}} = \frac{(|u-w|+c_s)\Delta x}{2}. \tag{180}$$

For subsonic flows, the gain of using a moving Lagrangian or ALE mesh is not significant. However, for supersonic flows in which $u \gg c_s$, choosing a grid velocity close enough to the flow velocity (say with $|u-w| < c_s$) can significantly reduce the numerical diffusion. More importantly, the resulting diffusion parameter can be much more uniform than for an Eulerian scheme. This is true, for example, in a Keplerian disc; when the rotation velocity varies strongly with radius, so does the numerical diffusion of an Eulerian scheme. Lagrangian or ALE schemes have much more uniform diffusion properties throughout the disc.

The main limitation of ALE schemes arises in strong shearing flows like, for example, in a Keplerian disc or in a vortex. The mesh can be distorted so much that initially neighboring mesh points can drift apart, resulting in highly distorted cell faces and volume elements (see, e.g., Vilar et al. 2014). The classic technique to overcome severe mesh distortions is to remap the flow variables to a new, smoother mesh. The remeshing step can become quite cumbersome and also leads to an additional source of numerical diffusion, defeating the purpose of the ALE technique. A significant breakthrough in the MvM methodology was obtained recently by using a Voronoi tessellation to define cell faces around moving cell centroids. This naturally solves the problem of the apparition of singularities in the mesh topology in strong shearing flows. This led to the design of the AREPO code for astrophysical fluid flows (Springel 2010a).

A final note needs to be made on the accuracy of adaptive or MvMs. Although these two techniques have been designed to minimize numerical diffusion, it has been shown that large

inhomogeneities in the cell size can reduce the order of accuracy of the underlying numerical schemes compared with the original, Cartesian-grid Godunov techniques. This fact can be demonstrated using an ME analysis with a nonuniform mesh (Giles 1989, Holleman et al. 2013) in which exact cancellation of terms in the Taylor expansion that occur in a symmetrical Cartesian mesh is absent. For AMR codes, this effect leads to a first-order accurate scheme at coarse-fine boundaries for an otherwise second-order scheme far from boundaries. For unstructured meshes, with random, inhomogeneous cell shapes, this loss of accuracy can propagate to the entire computational volume (Katz & Sankaran 2011). This last property depends very sensitively on the mesh regularity and on the details of the underlying HD solver, so that it is very difficult to draw general conclusions for moving or ALE meshes. The message here is that for adaptive meshes, as well as for MvMs, numerical results in regions of strongly varying cell size (like, for example, close to a coarse-fine AMR boundary) must be considered with great care.

8. ASTROPHYSICAL FLUIDS SOFTWARE

With the ever increasing power of supercomputers and the easier access to national and international supercomputing time allocations, numerical HD has become much more popular and easy to perform. It is now quite customary to find observational or theory papers featuring advanced fluid simulations that are used to strengthen scientific results. A key aspect of astrophysical software development is in the availability of such codes to a large community of potential users. Over the past decade, this has led to the multiplication of publicly available packages that anybody can download from the web and use as a simulation tool for astrophysical applications.

This strong evolution in our community is due to a change in our methodology. This is often discussed in the context of the general scientific methodology, which, in physics, is traditionally based on reproducible experiments, on one hand, and on mathematically sound but falsifiable theories, on the other hand. The reproducibility of the experiment and the detailed publication of the experimental apparatus are the heart of the scientific methodology for experiments, whereas pure logical reasoning is validating (or invalidating) the mathematical derivation for theories. Numerical simulations are in between these two classic approaches. Although there is a clearly identified algorithm, which could be described as a set of mathematical relations that is subject to pure logic, the algorithm is turned into a code in which many dirty details cannot be described as a set of logical instructions. Moreover, an actual simulation is interpreted as a numerical experiment, which should also be reproducible even if not by other codes but at least by different users using the same code. The reproducibility of the numerical experiment is therefore at the core of the scientific methodology, which is precisely why making simulation software publicly available is so important. In other words, when simulation results are published, it is mandatory to make the code immediately available to the community so that the entire process can be considered "scientific" and so experts in the field can reproduce the experiment using competing codes as well as the original code.

Fortunately, there is in astrophysics a long tradition of publicly available software, starting with the precursor, ZEUS (Stone & Norman 1992), and leading now to a wealth of very powerful and easy to use tools. A short overview of a nonexhaustive list of these software programs is given here, but the reader is encouraged to consult the public repository of astrophysics software **http://www.ascl.net**, using the search keyword "hydro". The most versatile codes are probably the ones based on the AMR technique, because it allows performing simple, Cartesian grid simulations but also adaptively refined grid simulations, allowing the very large dynamical range often required in self-gravity calculations. The `ENZO` code is a good example of large community codes that can

feature, beyond a pure HD scheme, MHD and relativistic HD solvers coupled to ray-tracing schemes for radiation and various Poisson solvers (Bryan et al. 2014). It has been developed since the late nineties for cosmology problems and has been quite successful in the past decade in addressing (among others) the problem of the formation of the first stars (Abel et al. 2002). Two other AMR codes have been developed for cosmology, galaxy, and star-formation applications, namely the RAMSES code (Teyssier 2002, Fromang et al. 2006) and the ART code (Kravtsov et al. 1997). These different codes are highly complementary, because ENZO is based on a patch-based AMR strategy, using large rectangular grids optimally placed in the flow, whereas RAMSES and ART are based on an octree AMR structure. As an example of the versatility of these codes, we report on various simulations performed with the RAMSES code, from large-scale cosmological simulations (Teyssier et al. 2009), some of them with a modified gravity model (Li et al. 2012), and galaxy formation simulations (Agertz et al. 2011) as well as studies of the magnetized collapse of molecular clouds (Hennebelle & Teyssier 2008) and more recently relativistic HD (Lamberts et al. 2013) and RT calculations (Commercon et al. 2011b, Rosdahl et al. 2013). In the context of Type Ia supernovae explosions, the FLASH code was developed by a large group of experts in compressible, reactive flows and was probably the first massively parallel AMR code ever developed in astrophysics (Fryxell et al. 2000). It has been used mostly for stellar explosions simulations (Jordan et al. 2008) as well as for galaxy clusters (Yang et al. 2009) and protostellar cores simulations (e.g., Banerjee & Pudritz 2006). The recent decade has seen the advent of many novel MHD solvers, following the methodology described earlier in this review. The NIRVANA code was probably the first full AMR MHD code in astrophysics (Ziegler 1998, 2005), and it was based on the constrained transport technique. Modern, higher-order MHD codes have been developed recently, such as the ATHENA code (Stone et al. 2008) and the PLUTO code (Mignone et al. 2007). Note that the ATHENA code is also featuring the VET technique for RHD (see Section 5). The PLUTO code has also the interesting feature of being able to deal with cylindrical and spherical grids using a weighted ENO (WENO) higher-order scheme. Finally, last but not least, let us mention the AREPO code, which is based on both MvM and AMR techniques by Springel (2010a) and has been already applied to galaxy formation. This last code, because it is so recent, is unfortunately not public yet.

These different codes are all based on different techniques and are usually quite popular in different communities. It is therefore difficult to justify using only one code rather than another. Experience in using these tools is building up slowly inside very active user communities; currently, social or historical justifications are still usually stronger than accuracy or performance considerations. Nevertheless, the concepts discussed in this review apply equally to all these software packages. A higher-order technique in one code may be less diffusive than a lower-order one in another, but close to flow discontinuity all schemes are usually very diffusive. Different codes are coupling the HD equations to the source terms (gravity, cooling, chemistry) quite differently, because these routines have been developed for very different applications. For example, higher-order Godunov methods are very efficient for moderate Mach number flows, but may eventually break for very high Mach numbers. Great care must be taken when using a code outside its traditional comfort zone. The various techniques discussed in this review will be helpful for a new user in assessing the quality of numerical HD simulations.

DISCLOSURE STATEMENT

The author is not aware of any affiliations, memberships, funding, or financial holdings that might be perceived as affecting the objectivity of this review.

ACKNOWLEDGMENTS

I thank my students, collaborators, and friends, who helped me develop many new computational tools and, more importantly, new ideas over the past decade. I would not have been able to write this review without them. I am also thankful to the anonymous referee, who did a tremendous job in improving the quality of the manuscript.

LITERATURE CITED

Abel T, Bryan GL, Norman ML. 2002. *Science* 295:93–98
Abel T, Norman ML, Madau P. 1999. *Ap. J.* 523:66–71
Abel T, Wandelt BD. 2002. *MNRAS* 330:L53–56
Agertz O, Teyssier R, Moore B. 2011. *MNRAS* 410:1391–408
Altay G, Croft RAC, Pelupessy I. 2008. *MNRAS* 386:1931–46
Aubert D, Teyssier R. 2008. *MNRAS* 387:295–307
Baek S, Di Matteo P, Semelin B, Combes F, Revaz Y. 2009. *Astron. Astrophys.* 495:389–405
Balbus SA, Henri P. 2008. *Ap. J.* 674:408–14
Balsara DS, Dumbser M, Abgrall R. 2014. *J. Comput. Phys.* 261:172–208
Banerjee R, Pudritz RE. 2006. *Ap. J.* 641:949–60
Berger MJ, Colella P. 1989. *J. Comput. Phys.* 82:64–84
Berger MJ, Oliger J. 1984. *J. Comput. Phys.* 53:484–512
Berthon C, Charrier P, Dubroca B. 2006. *J. Sci. Comput.* 31:347–89
Boscheri W, Dumbser M. 2014. *J. Comput. Phys.* 275:484–523
Bouchut F. 2004. *Nonlinear Stability of Finite Volume Methods for Hyperbolic Conservation Laws: And Well-Balanced Schemes for Sources*. Basel: Birkhäuser Verlag
Brackbill JU, Barnes DC. 1980. *J. Comput. Phys.* 35:426–30
Bryan GL, Norman ML. 1995. *Am. Astron.* 187:1421
Bryan GL, Norman ML, O'Shea BW, et al. 2014. *Ap. J. Suppl. Ser.* 211:19
Bryan GL, Norman ML, Stone JM, Cen R, Ostriker JP. 1995. *Comput. Phys. Commun.* 89:149–68
Calhoun D, LeVeque RJ. 2000. *J. Comput. Phys.* 157:143–80
Cantalupo S, Porciani C. 2011. *MNRAS* 411:1678–94
Cargo P, Gallice G. 1997. *J. Comput. Phys.* 136:446–66
Cen R. 2002. *Ap. J. Suppl. Ser.* 141:211–27
Ciardi B, Ferrara A, Marri S, Raimondo G. 2001. *MNRAS* 324:381–88
Cockburn B, Shu CW. 1998. *J. Comput. Phys.* 141:199–224
Colella P, Woodward PR. 1984. *J. Comput. Phys.* 54:174–201
Commercon B, Audit E, Chabrier G, Chièze JP. 2011a. *Astron. Astrophys.* 530:13
Commercon B, Teyssier R, Audit E, Hennebelle P, Chabrier G. 2011b. *Astron. Astrophys.* 529:35
Crockett RK, Colella P, Fisher RT, Klein RJ, McKee CI. 2005. *J. Comput. Phys.* 203:422–48
Dedner A, Kemm F, Kröner D, et al. 2002. *J. Comput. Phys.* 175:645–73
Enßlin T, Pfrommer C, Miniati F, Subramanian K. 2011. *Astron. Astrophys.* 527:99
Evans CR, Hawley JF. 1988. *Ap. J.* 332:659–77
Fromang S, Hennebelle P, Teyssier R. 2006. *Astron. Astrophys.* 457:371–84
Fromang S, Papaloizou J, Lesur G, Heinemann T. 2007. *Astron. Astrophys.* 476:1123–32
Fryxell B, Olson K, Ricker P, et al. 2000. *Ap. J. Suppl. Ser.* 131:273–334
Giles MB. 1989. In *Proc. 11th Int. Conf. Numerical Methods Fluid Dyn.*, ed. DL Dwoyer, MY Hussaini, RG Voigt, pp. 273–77. Berlin: Springer-Verlag
Glover SCO, Mac Low MM. 2007. *Ap. J. Suppl. Ser.* 169:239–68
Gnedin NY. 1995. *Ap. J. Suppl. Ser.* 97:231–57
Gnedin NY, Abel T. 2001. *New Astron.* 6:437–55
Godunov SK. 1959. *Mat. Sb.* 89:271–306
González M, Audit E, Huynh P. 2007. *Astron. Astrophys.* 464:429–35

Gottlieb D, Orszag SA, Sod GA. 1978. *J. Appl. Mech.* 45:969
Grassi T, Bovino S, Schleicher DRG, et al. 2014. *MNRAS* 439:2386–419
Harten A, Lax PD, van Leer B. 1983. *SIAM Rev.* 25:35–61
Hennebelle P, Teyssier R. 2008. *Astron. Astrophys.* 477:25–34
Hockney RW, Eastwood JW. 1988. *Computer Simulation Using Particles.* Bristol: Hilger
Holleman R, Fringer O, Stacey M. 2013. *Int. J. Numer. Methods Fluids* 72:1117–45
Hubbard ME. 1999. *J. Comput. Phys.* 155:54–74
Jiang GS, Wu CC. 1999. *J. Comput. Phys.* 150:561–94
Jiang YF, Stone JM, Davis SW. 2012. *Ap. J. Suppl. Ser.* 199:14
Jiang YF, Stone JM, Davis SW. 2014. *Ap. J. Suppl. Ser.* 213:7
Jordan GC IV, Fisher RT, Townsley DM. 2008. *Ap. J.* 681:1448
Joulain K, Falgarone E, Pineau des Forêts G, Flower D. 1998. *Astron. Astrophys.* 340:241–56
Jubelgas M, Springel V, Enßlin T, Pfrommer C. 2008. *Astron. Astrophys.* 481:33–63
Käppeli R, Mishra S. 2014. *J. Comput. Phys.* 259:199–219
Katz A, Sankaran V. 2011. *J. Comput. Phys.* 230:7670–86
Kim J, Balsara DS. 2014. *J. Comput. Phys.* 270:634–39
Klein RI, McKee CF, Colella P. 1994. *Ap. J.* 420:213–36
Knebe A, Green A, Binney J. 2001. *MNRAS* 325:845–64
Kravtsov AV, Klypin AA, Khokhlov AM. 1997. *Ap. J. Suppl. Ser.* 111:73
Krumholz MR, Klein RI, McKee CF, Bolstad J. 2007. *Ap. J.* 667:626–43
Lamberts A, Fromang S, Dubus G, Teyssier R. 2013. *Astron. Astrophys.* 560:79
Lesur G, Kunz MW, Fromang S. 2014. *Astron. Astrophys.* 566:56
LeVeque RJ. 1992. *Numerical Methods for Conservation Laws*. Basel: Birkhäuser Verlag. 2nd ed.
Levermore CD. 1984. *J. Quant. Spectrosc. Radiat. Transf.* 31:149–60
Li B, Zhao G-B, Teyssier R, Koyama K. 2012. *J. Cosmol. Astropart. Phys.* 01(2012):051
Liu TP. 1987. *Commun. Math. Phys.* 108:153–75
Londrillo P, del Zanna L. 2004. *J. Comput. Phys.* 195:17–48
Lowrie RB, Morel JE, Hittinger JA. 1999. *Ap. J.* 521:432–50
Majda A. 1984. *Compressible Fluid Flow and Systems of Conservation Laws in Several Space Variables.* New York: Springer
McCorquodale P, Colella P. 2011. *Commun. Appl. Math. Comput. Sci.* 6:1–25
Mellema G, Iliev IT, Alvarez MA, Shapiro PR. 2006. *New Astron.* 11:374–95
Mignone A, Bodo G, Massaglia S, et al. 2007. *Ap. J. Suppl. Ser.* 170:228–42
Mihalas D, Mihalas BW. 1984. *Foundations of Radiation Hydrodynamics.* New York: Oxford Univ. Press
Miyoshi T, Kusano K. 2005. *J. Comput. Phys.* 208:315–44
Mocz P, Vogelsberger M, Hernquist L. 2014. *MNRAS* 442:43–55
Murphy JW, Burrows A. 2008. *Ap. J. Suppl. Ser.* 179:209–41
Nakamoto T, Umemura M, Susa H. 2001. *MNRAS* 321:593–604
Nool M, Keppens R. 2002. *Comput. Methods Appl. Math.* 2:92–109
Pakmor R, Springel V. 2013. *MNRAS* 432:176–93
Pawlik AH, Schaye J. 2008. *MNRAS* 389:651–77
Pawlik AH, Schaye J. 2011. *MNRAS* 412:1943–64
Pen UL. 1998. *Ap. J. Suppl. Ser.* 115:19–34
Petkova M, Springel V. 2011. *MNRAS* 415:3731–49
Powell KG, Roe PL, Linde TJ, Gombosi TI, De Zeeuw DL. 1999. *J. Comput. Phys.* 154:284–309
Press WH, Teukolsky SA, Vetterling WT, Flannery BP. 1992. *Numerical Recipes in C: The Art of Scientific Computing.* New York: Cambridge Univ. Press. 2nd ed.
Razoumov AO, Cardall CY. 2005. *MNRAS* 362:1413–17
Rijkhorst EJ, Plewa T, Dubey A, Mellema G. 2006. *Astron. Astrophys.* 452:907–20
Rosdahl J, Blaizot J, Aubert D, Stranex T, Teyssier R. 2013. *MNRAS* 436:2188–231
Rybicki GB, Lightman AP. 1986. *Radiative Processes in Astrophysics.* Hoboken, NJ: Wiley-VCH
Ryu D, Ostriker JP, Kang H, Cen R. 1993. *Ap. J.* 414:1–19
Schmidt W, Federrath C. 2011. *Astron. Astrophys.* 528:106

Schmidt W, Niemeyer JC, Hillebrandt W. 2006. *Astron. Astrophys.* 450:265–81
Shu CW, Osher S. 1988. *J. Comput. Phys.* 77:439–71
Shu FH. 1992. *The Physics of Astrophysics*, Vol. II: *Gas Dynamics*. Mill Valley, CA: Univ. Sci. Books
Skinner MA, Ostriker EC. 2013. *Ap. J. Suppl. Ser.* 206:21
Spitzer L Jr, Härm R. 1953. *Phys. Rev.* 89:977
Springel V. 2010a. *MNRAS* 401:791–851
Springel V. 2010b. *Annu. Rev. Astron. Astrophys.* 48:391–430
Stone JM, Gardiner TA, Teuben P, Hawley JF, Simon JB. 2008. *Ap. J. Suppl. Ser.* 178:137–77
Stone JM, Mihalas D, Norman ML. 1992. *Ap. J. Suppl. Ser.* 80:819–45
Stone JM, Norman ML. 1992. *Ap. J. Suppl. Ser.* 80:753–90
Stone JM, Norman ML. 1992. *Ap. J. Suppl. Ser.* 80:791
Suresh A, Huynh HT. 1997. *J. Comput. Phys.* 136:83–99
Susa H. 2006. *Publ. Astron. Soc. Jpn.* 58:445–60
Teyssier R. 2002. *Astron. Astrophys.* 385:337–64
Teyssier R, Pires S, Prunet S, et al. 2009. *Astron. Astrophys.* 497:335–41
Titarev VA, Toro EF. 2002. *J. Sci. Comput.* 17:609–18
Toro EF. 1999. *Riemann Solvers and Numerical Methods for Fluid Dynamics*. Berlin: Springer-Verlag
Tóth G. 2000. *J. Comput. Phys.* 161:605–52
Truelove JK, Klein RI, McKee CF, et al. 1997. *Ap. J. Lett.* 489:L179
van Leer B. 1976. In *Computing Plasma Physics Astrophysics*, ed. D Biskamp, p. 1. Amsterdam: North-Holland
Vilar F, Maire PH, Abgrall R. 2014. *J. Comput. Phys.* 276:188–234
Whalen D, Norman ML. 2006. *Ap. J. Suppl. Ser.* 162:281–303
Wise JH, Abel T. 2011. *MNRAS* 414:3458–91
Woodward PR, Herwig F, Lin PH. 2015. *Ap. J.* 798:49–65
Yang H, Ricker PM, Sutter PM. 2009. *Ap. J.* 699:315–29
Ziegler U. 1998. *Comput. Phys. Commun.* 109:111–34
Ziegler U. 2005. *Astron. Astrophys.* 435:385–95
Zienkiewicz OC. 1971. *The Finite Element Method in Engineering Science.* New York: McGraw-Hill. 2nd ed.